*Ecological Applications*, 16(4), 2006, pp. 1421–1435


# SONAR BACKSCATTER DIFFERENTIATION OF DOMINANT MACROHABITAT TYPES IN A HYDROTHERMAL VENT FIELD

Sébastien Durand,[1,2,3] Pierre Legendre,[1] and S. Kim Juniper[2]

[1]*Département de Sciences Biologiques, Université de Montréal, C.P. 6128, Succursale Centre-ville, Montréal, Québec, Canada H3C 3J7*
[2]*GEOTOP, Université du Québec à Montréal, C.P. 8888, Succursale Centre-ville, Montréal, Québec, Canada H3C 3P8*

*Abstract*. Over the past 20 years, sonar remote sensing has opened ways of acquiring new spatial information on seafloor habitat and ecosystem properties. While some researchers are presently working to improve sonar methods so that broad-scale high-definition surveys can be effectively conducted for management purposes, others are trying to use these surveying techniques in more local areas. Because ecosystem management is scale-dependent, there is a need to acquire spatiotemporal knowledge over various scales to bridge the gap between already-acquired point-source data and information available at broader scales. Using a 675-kHz single-pencil-beam sonar mounted on the remotely operated vehicle ROPOS, 2200 m deep on the Juan de Fuca Ridge, East Pacific Rise, five dominant habitat types located in a hydrothermal vent field were identified and characterized by their sonar signatures. The data, collected at different altitudes from 1 to 10 m above the seafloor, were depth-normalized. We compared three ways of handling the echoes embedded in the backscatters to detect and differentiate the five habitat types; we examined the influence of footprint size on the discrimination capacity of the three methods; and we identified key variables, derived from echoes that characterize each habitat type. The first method used a set of variables describing echo shapes, and the second method used as variables the power intensity values found within the echoes, whereas the last method combined all these variables. Canonical discriminant analysis was used to discriminate among the five habitat types using the three methods. The discriminant models were constructed using 70% of the data while the remaining 30% were used for validation. The results showed that footprints 20–30 cm in diameter included a sufficient amount of spatial variation to make the sonar signatures sensitive to the habitat types, producing on average 82% correct classification. Smaller footprints produced lower percentages of correct classification; instead of the habitat types, the sonar data responded to intrapatch roughness and hardness characteristics. The sonar variables used in this study and the methods for extracting and transforming them are fully described in this paper and available in the public domain.

*Key words: canonical discriminant analysis; habitat types; hydrothermal vents; Juan de Fuca Ridge; remotely operated vehicle (ROV); remote sensing; sonar backscatter.*

## Introduction

Broad-scale remote-sensing surveys have brought many benefits to agriculture, mineral exploration, and environmental management in the terrestrial environment. In the field of landscape ecology, satellite imagery, airborne photography, hyper-spectral imagery, passive/active microwaves, radar, lidar systems, and so forth provide information on habitat distribution, evolution, connectivity, structuring process, recovery rates, as well as evaluation of transition zones, metapopulations, and even plant population physiological status such as stress level (Lee and Chough 2001, Carey et al. 2003, Hewitt et al. 2004, Kotchenova et al. 2004, Lee and Anagnostou 2004, Moya et al. 2004, Schmidtlein and Sassin 2004). However, because seawater is relatively opaque to electromagnetic waves (Foster-Smith and Sotheran 2003), optical and radio frequency remote-sensing tools find few applications in ecological studies and habitat management on the deep ocean floor. Considering that more than 60% of the Earth's surface is covered by 1000 m or more of water, the lack of efficient investigation tools constitutes not only a serious obstacle to understanding the dynamics of biodiversity and ecosystem functioning at a global scale, but also impairs our capacity to correctly manage deep-sea resources. On the rare occasions in which towed platforms and research submersibles reach such depths, mounted video and still cameras can be used to survey organism distributions and, at smaller scales, to obtain direct estimates of benthic organism density, microtopography, and substrate characteristics. However, the spatial scope and resolving power of light-based systems remains very limited in what is essentially an aphotic and light-absorbing (i.e., turbid) environment. Consequently, detailed optical imaging of the deep seabed must be

Manuscript received 28 February 2005; revised 2 August 2005; accepted 21 August 2005; final version received 12 December 2005. Corresponding Editor: D. S. Schimel.
[3] E-mail: Sebastien.Durand@umontreal.ca

conducted at very slow speeds and can rarely be done from altitudes that would provide optimal spatial resolution (Parry et al. 2003, in situ experimentation). Benthic ecologists have long awaited the development of efficient remote-sensing techniques that could be applied from a distance over large areas of the deep ocean floor (Hewitt et al. 2004). Even with the recent advances in light-based and laser-line systems (Irish and Lillycrop 1999, Carey et al. 2003) developed for shallow environments such as the coastal zone, acoustic technology remains the only method that has the potential to carry information through ultimately thousands of meters of water. Acoustic data also lend themselves much more easily to automated mapping and statistical analyses than do maps produced from underwater cameras.

Acoustic sounders and later-developed multibeam sonars have been used extensively for precise, broad-scale mapping of seafloor topography. More recently, innovations in sonar technology have allowed researchers to demonstrate the potential for accurate mapping of seafloor habitat characteristics at broad scales. Through established methods (Burns et al. 1989, Chivers et al. 1990, Prager et al. 1995, Clarke and Hamilton 1999, Burczynski 2001, Hamilton 2001, Ellingsen et al. 2002, Legendre et al. 2002), commercially available systems, such as BioSonics' VBT, Echoview, QTC VIEW, or RoxAnn, are now used by researchers to extract habitat information from returning acoustic signals. One line of current research is the development of effective methods to cover large areas that would involve making the footprint of the sonar beam (sample area) large enough to reduce extrapolation needs. This would, however, result in loss of information on microscale habitat heterogeneity, which is of great importance for community ecology and for maintenance of biodiversity. Understanding ecological dynamics and managing ecosystems require the ability to effectively map broad expanses, as well as an understanding of smaller-scale ecosystem features, which quite often play a determining role at broader scales.

Using only acoustic spectral features, Pace and Gao (1988) successfully classified six seabed types: sand, mud, clay, gravel, stone, and rock. Today, the most commonly used method is to use a side-scan sonar using frequencies of ~1–200 kHz to detect the substratum type through the use of backscatter intensity curves and texture analysis of side-scan images (e.g., Brown et al. 2002, Zajac et al. 2003, Hewitt et al. 2004). But there has been little methodological development for backscatter interpretation at the higher acoustic frequencies that could distinguish seafloor habitats and macrofaunal communities.

This paper begins this methodological development by experimenting with acoustic returns from a high-frequency sonar, in order to address the following questions: (1) Is the information found within backscatters informative enough to allow accurate discrimination of abyssal benthic habitats, in this particular case, five hydrothermal habitats within a vent field ecosystem? (2) If so, does increasing footprint size allow the acquisition of backscatters that are increasingly representative of the spatial heterogeneity inherent to each habitat? (3) Can we find specific sets of variables that could be used to correctly identify the nature of the habitat surveyed, based on sonar signatures?

## Materials and Methods

Acoustic information was obtained during dives of the remotely operated vehicle (ROV) ROPOS in 2001 and 2002. Dives were conducted during cruises of the Canadian Coast Guard Ship J.P. Tully to the hydrothermal fields of the Endeavour Segment of the Juan de Fuca Ridge in the northeast Pacific Ocean, 300 km southwest of Vancouver Island. Acoustic data were obtained using an Imagenex 881B single-beam sonar, equipped with a subminiature profiling head unit model 881–000–130 (Imagenex Technology, Port Coquitlam, British Columbia, Canada) using 675-kHz frequency and a 1.7° pencil beam width, mounted on the submersible. Subsea positioning was determined using a long baseline (LBL) acoustic navigation system (Teledyne Benthos, North Falmouth, Massachusetts, USA) that included a PS8010 Edgetech transceiver (Edgetech, West Wareham, Massachusetts, USA) and five bottom transponders georeferenced using the vessel's dynamic GPS system. All interrogation, receiving, and processing related to this LBL system was handled through the Seascape and Workboat software (Software Engineering Associates, Seattle, Washington, USA) on the support vessel.

For all the local navigation and ground-truthing procedures, images from the submersible's low-light, silicon-intensified targeting (SIT) camera, as well as a three charge-coupled device (3-CCD) color video were recorded on S-VHS or digital (mini-digital video) tapes for post-processing (mainly habitat identification and transect filtering).

To transform and statistically analyze the collected sonar information, we developed functions under R-project version 2.1.0 (R Development Core Team 2005). R is a statistical language freely downloadable from the Internet.

### *Study site and habitat description*

Located 2200 m deep on the Endeavour Segment of Juan de Fuca Ridge (47°57′47″ N, 129°05′30″ W), Clambed is a hydrothermal vent field of ~50 × 20 m with a central, actively venting chimney (named "Hershey") standing 2–3 m tall and surrounded by localized diffuse venting. Covered mostly by broken lava flows and nearly sediment-free, the site's overall topography consists of two roughly parallel 2–3 m high north/south trending ridges colonized by hydrothermal vent tubeworms (*Ridgeia piscesae*; see Plate 1) and polychaete/limpet assemblages (*Paralvinella palmiformis, Paralvinella sulfincola*)/(*Lepetodrilus fucensis*). Between the ridges,

PLATE 1. Glimpses of the habitat at the Clam and Tube sites. (Left) Two spider crabs feed within a community of clams and scattered tubeworms. (Right) A high-density colony of the same species of tubeworm, *Ridgeia piscesae*. These tubeworms can grow to 2 m long. Photo credit: S. Durand.

lightly sedimented depressions are found, which host small communities of vesicomyid clams (*Calyptogena* cf. *pacifica*), another hydrothermal vent species. Based on previous sightings of the studied vent field and on work on Juan de Fuca Ridge hydrothermal species assemblages by Sarrazin and Juniper (1999), five visually distinct and dominant habitats were selected to be probed in situ. In Fig. 1, a photograph of each habitat is associated with a sample sonar signature (first echo only).

1. *Ridge top with dense, continuous tubeworm bushes (habitat code: Tube)*.—Within this key habitat, the structure complexity of the dense tubeworm communities has been hypothesized to be a leading factor in diversity (Tsurumi and Tunnicliffe 2003). The channeling effect that tubeworm communities have on the hydrothermal fluid might reduce the environmental chemical and thermal fluctuations, just as the wind or temperature fluctuations are buffered in a terrestrial forest habitat. Within this microcosm, tubeworms can either serve as food source, refuge, or substratum, or as hunting ground. Easy to distinguish from the other habitat types, these dense, white, bush-like structures are often covered by microbial mats (e.g., *Arcobacter* sp. and *Folliculina* sp.; Wirsen et al. 2002, Léveillé and Juniper 2003) and host many small worms and gastropods (e.g., *Lepidonotopodium piscesae*, *Paralvinella dela*, *Paralvinella palmiformis*, and *Depressigyra globulus*) and squat lobsters (*Munidopsis alvisca*). Species residing within the tubeworm bushes are rarely visible in the video recordings.

2. *Ridge top with semi-continuous tubeworm bushes (habitat code: Peri)*.—Found at the boundary of dense tubeworm bushes, this habitat exhibits low tube densities and is the most visually diverse of the five habitats selected. Species found both outside and inside the tubeworm colonies can be seen in recorded imagery. The substratum is clearly visible over ~50% of the area.

3. *Ridge top without tubeworms (habitat code: Lava)*.—This habitat is the most common of all five habitats studied, and it consists of bare to lightly sedimented broken basaltic flow sheets. It is colonized by very low densities of species non-endemic to hydrothermal vents, such as unidentified holothurians, starfish, sponges, anemones, and a few crinoids.

4. *Ridge top with polychaete/limpet assemblages (habitat code: Limp)*.—Usually located in the immediate vicinity of visibly intense hydrothermal flow emissions, these highly localized and dense communities of limpets and polychaetes can completely cover the underlying substratum. Some polychaetes (e.g., *Lepidonotopodium piscesae* and *Branchinotogluma grasslei*) can be seen attached to the small tubes and shells of *Paralvinella palmiformis*, *Paralvinella sulfincola*, and *Lepetodrilus fucensis*.

5. *Sedimented depression with clams (habitat code: Clam)*.—Within the most sedimented sections of Clambed, a mixture of clams, empty shells, and a few fallen tubeworm tubes occur in sediment patches often visited by spider crabs (*Macroregonia macrochira*).

### *Study design*

In a pilot study (Durand et al. 2002), we showed that sonar signatures were sensitive enough to differentiate geological and biological features based on their respective densities, textures, and structures. To pursue the assessment of the use of sonar signatures as a remote-sensing tool requires some basic assumptions to be made: (1) Local water variations in chemistry, temperature, and amount of suspended particles did not significantly influence backscatters. (2) The ROV

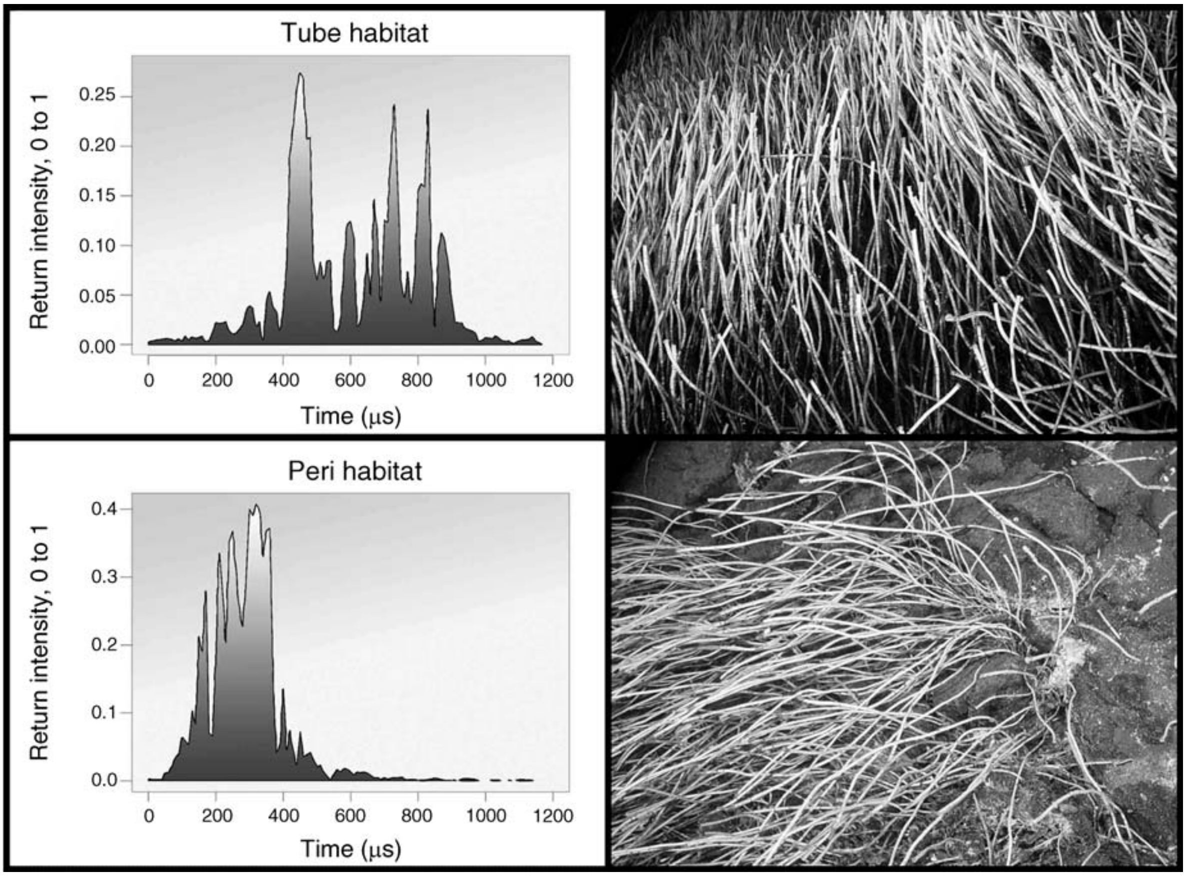


FIG. 1. Sample echo signatures at an altitude of 8.5 m (left), corresponding to the habitat types pictured on the right. To represent the sample echo signatures, only the first echoes of the backscatters were used here; the first and second echoes are described in Fig. 2. The selected habitats are located 2200 m deep on the Endeavour Segment of Juan de Fuca Ridge in the northeast Pacific Ocean.

submarine noises, gear, or transponder sonar installations did not interfere with the sonar acquisition process. (3) For every acquired backscatter, the area of seafloor receiving the sonar interrogation ping was horizontal and flat (Clarke and Hamilton 1999).

To assess the discrimination power of our sonar system, sonar data were collected at different altitudes from 1 to 10 m above the seafloor, using vertical transects. At least three vertical transects representing each habitat were taken at different locations in the field. With the sonar head always pointing straight down (at zero degree angle), each vertical transect started in a stable and controlled position with the ROV resting on top of the selected site. After a short acquisition period, henceforth referred to as the stable section, a slow and controlled vertical ascent was instigated. During sonar acquisition, both the SIT and color video cameras were recording. Once beyond 5 m of altitude, the pilot increased the submarine ascent speed to minimize unwanted horizontal drifting. Drifting is caused in part by the increased speed of horizontal currents as the submersible rises above the seafloor; it is also a direct consequence of visibility deterioration with altitude, which interferes with piloting. Using reference points such as key geological structures and other objects visually identified at the beginning of each transect recording, the transect positioning and good visibility could be ensured only until an altitude of 10 m. None of the data acquired beyond this altitude limit were used since the positioning was too uncertain and prone to error. A total of 18 vertical transects were acquired, with a mean duration of 4.5 min and ~670 sonar pings per transect. In 52 min 53 s of raw recording, 7761 backscatters were recorded in digital form with a mean sampling interval of 0.41 s, within the 1–10 m altitude range.

## SIGNAL PROCESSING METHODS

### *Visual filtering and data treatments*

With the footprints localized on SIT video frames, each sonar transect was visually filtered. Transect segments in which the footprints were outside the targeted habitat and frames with poor visibility were eliminated. Using an algorithm developed for this research and described in the next two subsections, the

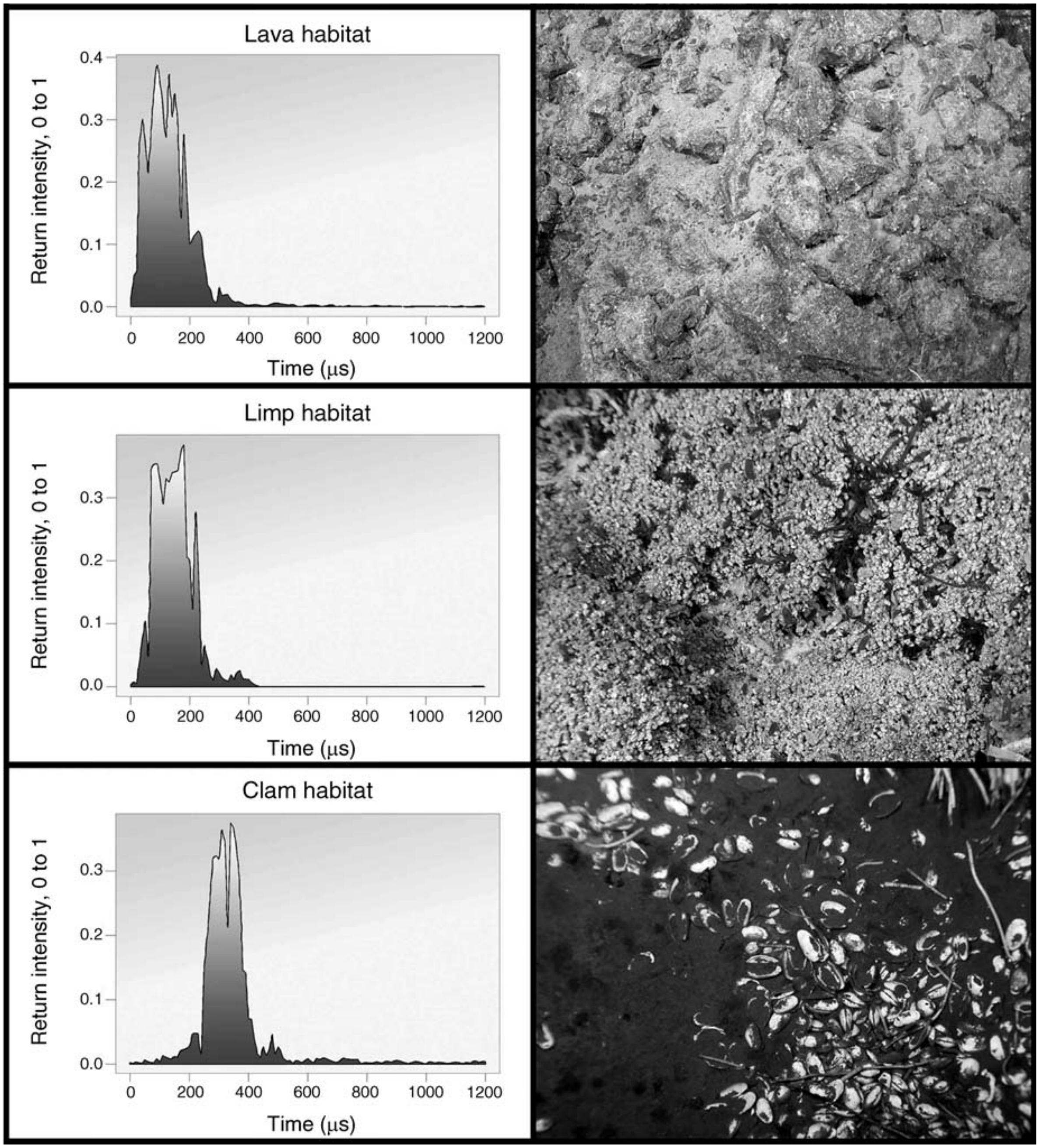


FIG. 1. Continued.

raw backscatters of the retained transect portions were analyzed. The beginning of the first echo was located by scanning the backscatters for their first substantial intensity increase. These areas were then used to estimate the sonar head acquisition altitude during sampling; Fig. 2 describes how the backscatters were segmented. Using these altitude estimates, a filtering procedure was initiated to identify and remove any other obviously bad signals carrying incomplete echoes or erroneous intensity curves. To detect and locate the first and second echoes (Fig. 2) inside a backscatter, both the original and smoothed backscatters were used; the smoothing algorithm used a moving window averaging 21 consecutive intensity values. We removed any acoustic return for which detection of either the first or second echo failed. For the remaining 7646 acoustic returns, we subtracted from the whole echo the signal ambient noise, averaged from the noise estimation areas. For logistic reasons, the recording of a large number of the echoes stopped within the second echo set area. As a

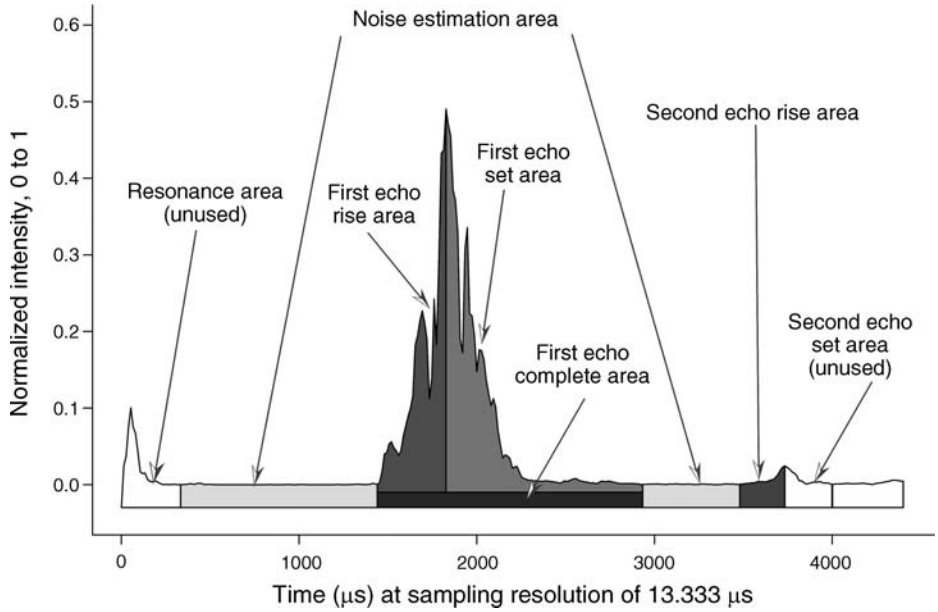


FIG. 2. Echo segmentation of a real backscatter, acquired at 1.28 m of altitude, for which intensities have only been filtered for noise. The intensity variables described in Fig. 3 come from the first echo complete area. The other variables were extracted using both the first and second echoes.

result, derived variables that express proportions between the first and second echoes consider only the second echo rise area.

Since our data were acquired at different altitudes, to compare echoes with one another, a depth normalization procedure was applied to correct both the strength of the recorded intensity values and the temporal spreading of the backscatters (Clarke and Hamilton 1999, Hamilton 2001). Note that since the sonar beam is a cone, the size of the sampled area, or footprint, is physically linked to the acquisition altitude. Therefore, even with depth normalization that accounts for temporal spreading and power, it is not possible to compensate for the effect of insonifying a large vs. a small habitat area. To assess the impact of such variation, altitude-dependent data tables, described below, were extracted and analyzed.

### *Sonar variable extraction methods*

Three approaches were used to extract variables from backscatters. The first approach is similar to the methods used in the QTC VIEW, RoxAnn, and BioSonics software. We computed a series of variables from both the first and second echo sections of all depth-normalized backscatters, producing a data table of 28 extracted variables referred to as VE (not shown), describing locations, sections, or proportions of areas. These variables are described in Appendix A (Table A1).

The second method used only the intensities of the first echo as variables. Once depth normalization was applied, the associated temporal correction stretched or compressed the individual acoustic returns. Intensities had originally been recorded at 13.333-μs intervals; the intensities making up the first echo were resampled with a 10-μs sampling interval, after smoothing using the "interspline" function of the R language (R::package::splines::interspline). Using these equally spaced intensity values, we created our intensity variables (Int) by averaging sets of five consecutive values, and we assembled them in a data table referred to as VI (not shown), which contained a maximum of 92 consecutive intensity variables per backscatter. For shorter echoes not producing 92 variables, zeros filled the empty cells. The third method combined all the variables found in VE and VI into a new data table called VT.

In Fig. 3, each box plot gives a descriptive insight into the role of the first 30 intensity variables used in the VI and VT data tables. By combining the box plot positions and the mean and median lines, it is possible to visually characterize the variables. The variables averaged from the corresponding intensity groups 1–5, 6–10, and 11–15, called "Int1–5," "Int6–10," and "Int11–15," respectively, clearly represent the rising portion of the echoes. Variables "Int16–20" and "Int21–25" describe the first echo peak. The intensity values from 26 to 90 (intensity variables "Int26–30" to "Int86–90") correspond to the backscatter tail or set area of the first echo. Beyond that, the curve becomes flat and cannot be visually interpreted.

### *Data filtering, segmentation, and transformations*

In data tables VI, VE, and VT, any variable exhibiting no variation within either of our habitat types, as well as any variable showing very little variation, or fewer than 10 individual values differing from the mean, was removed. The first 59 variables were kept in data table

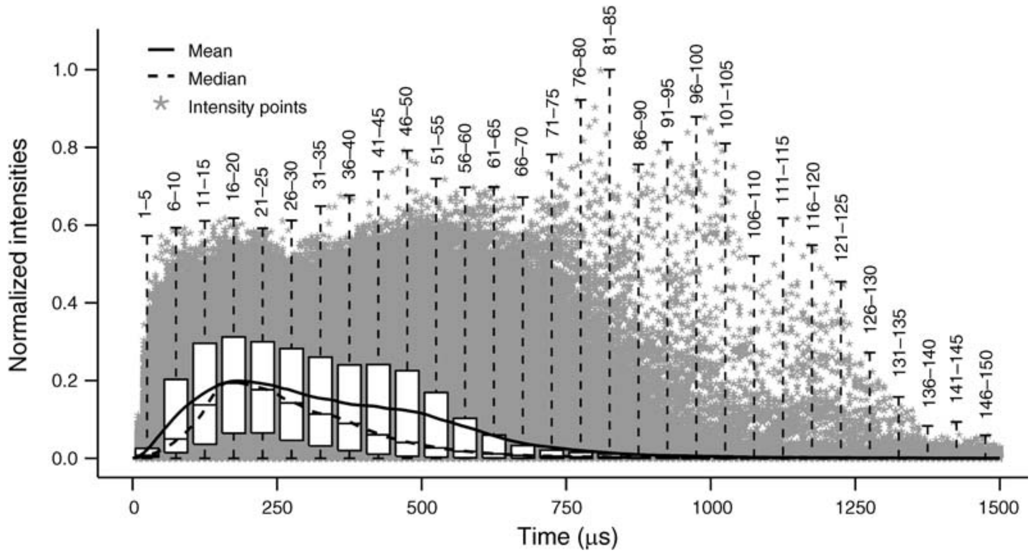


FIG. 3. A combination of the intensity values of all backscatters used in this study. The cloud of gray stars represents the first 150 intensity values found in the first echo of all acoustic returns. Each box plot portrays the localized distribution of five consecutive intensity values, which form one intensity variable. The whiskers of the box plots show the minimum and maximum values, while the boxes show subsection quartiles (25%, 50%, and 75%).

VI ("Int1–5" to "Int291–295"); 25 variables remained in data table VE after "Histo5" to "Histo7" had been removed (Appendix A: Table A1).

In order to bring the data tables close to the multinormality condition, which would improve the performance of discriminant analysis (see *Statistical analyses*), different transformations were applied to the VI and VE data tables prior to the creation of table VT. In data table VI, 15 possible transformations described in Table A2 of Appendix A were tried in turn on six different subtables. Because all variables found in data table VI are of the same nature (they represent signal intensities), they should all be subjected to the same transformation. To estimate the common skewness of all transects, we standardized the values of each variable within each transect, which controls for the effect of the first two moments of their distributions, and combined the standardized values in a single table. The absolute values of skewness were averaged across variables for each VI data table. The transformation that produced the smallest mean skewness was selected.

For data table VE, all variables were not of the same nature and did not have similar distributions. Therefore, for each variable we tested the following: no transformation, the square-root, the double square-root, or the log transformation and selected the transformation that produced the smallest skewness. After applying the best transformation to each variable, all variables found in the VI and VE sets were combined to create VT data tables.

For each of the resulting and newly transformed VI, VE, and VT data tables, five new subtables were created. Using only the backscatters found in the stable section (code STB, ~1 m altitude) of each transect, STB subtables were constructed for each habitat and used for control and initial tests. This application was restricted to the STB subtables because all their backscatters had been acquired during the period of greatest visibility, ensuring accurate habitat identification; altitude variations were also minimal so that the acquisition of returns was unaffected by depth-related phenomena (see Clarke and Hamilton 1999). Then, three altitude-related subtables were created using the following backscatter altitude acquisition ranges: 1–4 m, 4–7 m, and 7–10 m. Finally, for each of the five habitats, the backscatters found in the best altitude transect, in terms of visual sample quality and ROV displacement, were used to produce the BEST subtables. We then assessed the discriminating power of our three sets of variables found in the VI, VE, and VT data tables and the effect of altitude and footprint size by combining the information provided by the analysis of all these subtables.

### *Statistical analyses*

To assess the discriminating power of the sonar variables found in the VI, VE, and VT data tables, the percentage of correct classification (PCC) after discriminant analysis was computed using the function R-Pkg::MASS::predict.lda. For each data table, a random selection representing 70% of the backscatters was used the compute the discriminant model while the remaining 30% served to predict the habitat associated with each backscatter. The PCC index was calculated for these validation data.

For each data table, variance condensation was achieved by principal component analysis (PCA). We used only the principal components accounting for 99%

TABLE 1. Percentages of correct classification.

| Variable set and methods | Tables and subtables | | | | | | Mean |
|---|---|---|---|---|---|---|---|
| | STB | BEST | ALL | 1–4 | 4–7 | 7–10 | |
| VI | | | | | | | |
| COM | 85.4 | 69.9 | 58.7 | 63.1 | 63.0 | 72.4 | 68.8 |
| FWD | 79.6 | 71.0 | 58.1 | 61.3 | 61.7 | 73.1 | 67.5 |
| SEL | 83.8 | 71.6 | 58.6 | 62.8 | 63.3 | 76.9 | 69.5 |
| VE | | | | | | | |
| COM | 94.6 | 78.2 | 65.3 | 67.9 | 67.7 | 77.6 | 75.2 |
| FWD | 90.8 | 72.9 | 61.0 | 65.7 | 59.0 | 68.7 | 69.7 |
| SEL | 86.2 | 74.7 | 58.5 | 63.5 | 62.4 | 68.7 | 69.0 |
| VT | | | | | | | |
| COM | 95.8 | 78.8 | 68.0 | 70.7 | 76.6 | 85.1 | 79.2 |
| FWD | 94.4 | 76.9 | 63.4 | 68.7 | 65.5 | 76.9 | 74.3 |
| SEL | 94.1 | 75.5 | 63.6 | 70.4 | 68.4 | 84.3 | 76.1 |
| VI mean | 82.9 | 70.8 | 58.5 | 62.4 | 62.7 | 74.1 | 68.6 |
| VE mean | 90.5 | 75.3 | 61.6 | 65.7 | 63.0 | 71.7 | 71.3 |
| VT mean | 94.8 | 77.1 | 65.0 | 69.9 | 70.2 | 82.1 | 76.5 |
| Total mean | 89.4 | 74.4 | 61.7 | 66.0 | 65.3 | 76.0 | 72.1 |

*Notes:* Percentages of correct classifications (PCC) for the variable sets found in the intensity variables (VI), variables describing echo shapes (VE), and the combination of VI and VE (VT) data tables were estimated by three methods. The first analysis (COM) used the complete set of principal components accounting for 99% of the variance in the data. The second analysis (FWD) used only the original variables retained by forward selection. Finally, analysis SEL used eight VI, eight VE, or all of these 16 variables, depending on which variable set was tested. This variable selection was based on the distribution and frequency of the variables previously selected by forward selection. Analyses were repeated using the groups of returns that were obtained when the remotely operated vehicle (ROV) was stable and at low altitude (STB) or when they were found in the transects with the best sonar return quality (BEST). The other groups include sonar returns found in all vertical transects (ALL) or select those acquired at specific altitude ranges that are 1–4 m (1–4), 4–7 m (4–7), and 7–10 m (7–10). The selected habitats are located 2200 m deep on the Endeavour Segment of Juan de Fuca Ridge in the northeast Pacific Ocean.

of the variance (assembled in the COM data sets) in linear discriminant analyses (R-Pkg::MASS::lda) and obtained our first PCC results without selection of wave form variables; see Table 1.

Alternative strategies were also used. Firstly, instead of computing a PCA for each VI, VE, and VT data table, the variables with the highest contributions were identified by forward selection with permutation tests. A function to carry out discriminant analysis, following the algorithm described by ter Braak and Smilauer (2002: section 3.11) with forward selection of explanatory variables (ter Braak and Smilauer 2002: section 5.8.1), was developed in the R language by S. Dray (*personal communication*). Using only this selection of variables, henceforth referred to as FWD, discriminant analysis was computed again, producing another set of percentages of correct classification describing the discriminating power of a smaller set of selected variables for each of the three kinds of data tables (VI, VE, and VT). Secondly, since the set of selected variables varied from table to table, identical sets of variables had to be used in all tables to allow comparisons and understand the role of key variables. By choosing the variables with the highest selection frequencies in all FWD selections (Appendix A: Table A3), we created a subset of three variables called SEL. Discriminant analyses were computed with it, and a series of explanatory discriminant analysis plots were produced (Appendix B).

## RESULTS

Depth variation has been shown in the literature to affect our capacity to detect and differentiate sonar signatures (Hewitt et al. 2004). Without a proper depth normalization procedure, the effects of uncorrected altitude fluctuations are likely to overshadow the variation inherent in the nature of the seabed and fatally link the sonar signatures to altitude-related variables. To perform an accurate depth normalization, since the rate at which the sound is absorbed as it travels through water was estimated instead of being precisely measured, corrective measures were taken. To adjust the absorption rate and consequently optimize our depth normalization procedure, we used several plots such as those presented in Fig. 4 to visualize the effect of the power correction by comparing original to the power-normalized backscatters, respectively drawn in Fig. 4a and b. The thick and dark gray lines shown in both plots represent strong intensities and correspond to the first and second echo areas. In Fig. 4a, as the ROPOS gained altitude, the intensity of the backscatters weakened from left to right in all transects; consequently, paler grays are showing in the right-hand portion of each transect. In Fig. 4b, the power normalization algorithm removed the fading, to a point at which a homogeneous gray background was found, from left to right, within and among transects. The darker curves look more homogeneous; this is a visual sign of an accurate power correction (meaning as in Hamilton [2001]). Comparison

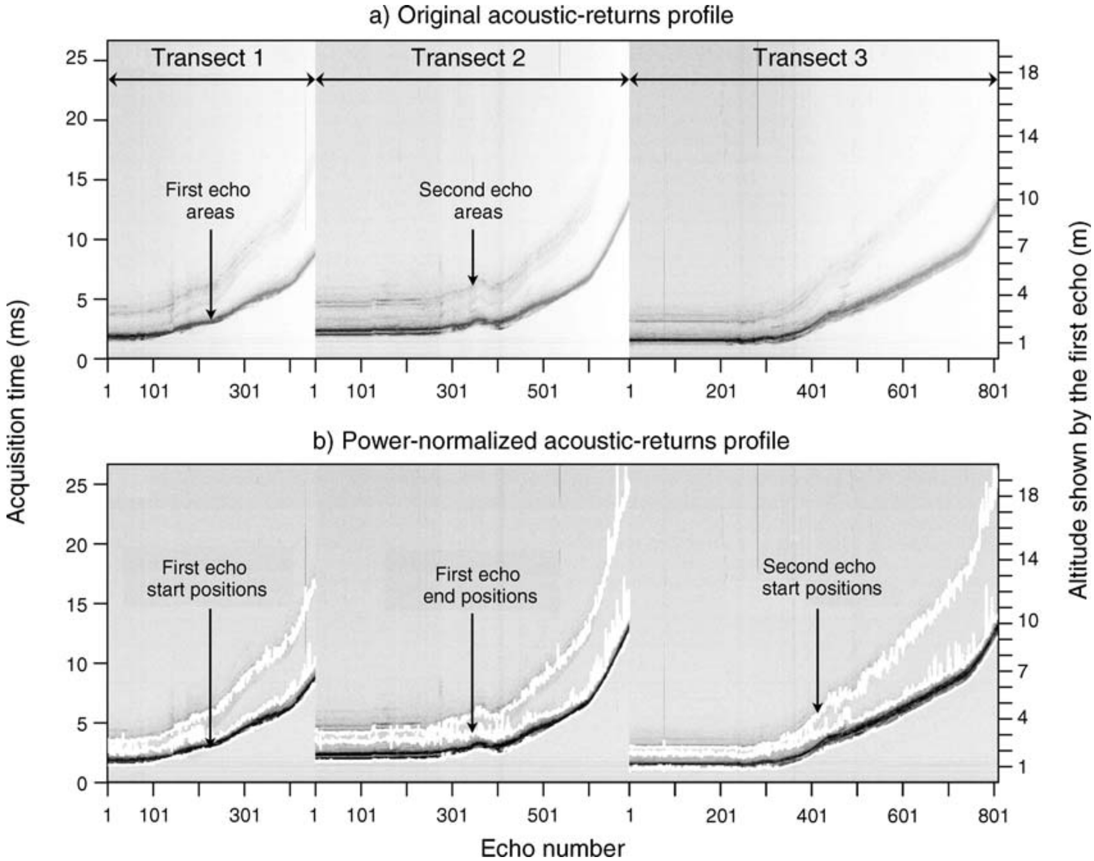


FIG. 4. (a) Original profiles of recorded acoustic returns. Echoes are represented by vertical lines of pixels going from the bottom to the top of the graph and shaded according to signal intensity (darker is stronger signal), for three vertical transects in the Peri habitat. The three dark curves are areas of strong intensities that correspond to the peaks of the first echoes. Above these three curves are three paler gray curves corresponding to the peaks of the second echoes. The rising shape of these lines, from left to right along each transect, is caused by the altitude gain. When the altitude increases, the delay between the time when the signal is sent and received for the first time by the sonar head also increases. Consequently, the resulting sonar signal intensity power is weaker because the longer it travels in water, the more it gets dissipated and absorbed. (b) The power-normalized acoustic returns are now uniform in shading. White lines show the boundaries of the first echoes and the second echo start positions, detected by the algorithm. The gray lines of the second echoes are mostly hidden by the white lines drawn over them. The second echo end positions are, in our case, the second echo maxima. The second echo end positions were not shown; they would have been barely distinguishable because they were too close to the second echo start positions.

of Fig. 4a and b shows that the power correction in the depth normalization procedure increased our capacity to visualize specific sections of the backscatters. (In Fig. 4b, the addition of three overlaid white lines to the intensity profiles describing the first echo start and end positions plus the second echo start positions served two purposes. First, they allowed us to visually assess the success of the echo detection algorithm; secondly, they served as visual markers showing from which sections of the backscatters we were extracting our variables.)

The first and second echo starting curves should, in principle, be smooth if the algorithm operates correctly, because the physical conditions under which the echoes were acquired involved slow and gradual ROV rise and constant recording. This is the case for the first echoes, but the detection of the beginning of the second echoes is more random. Instead of having the second echo bouncing off the seafloor to the air/water interface to the seafloor and finally to the sonar head, our second echoes are reflected on the seafloor, the underside of the ROV, and the seafloor again, before reaching the sonar head for the second time. Reflections from a large, homogeneous air/water interface are much smoother than reflections from the ventral surface of the ROV, which has an irregular shape, holes, and attached equipment such as canisters of various shapes, textures, and densities. In addition, because the second echoes are by nature weak, an accurate second echo detection algorithm was difficult to produce. More work will be necessary to improve this algorithm.

After extraction of the variables, normalizing transformations were applied to all data tables. Table A1 in Appendix A shows the VE variable names and gives the selected transformations and associated skewness val-

TABLE 2. Habitat assignments of all echoes based on the combination (VT) of intensity variables (VI) and variables describing echo shapes (VE) data tables, using the complete variable sets (COM).

| Habitat observed, by altitude | Habitat assigned by sonar | | | | | Partial PCC |
|---|---|---|---|---|---|---|
| | Tube | Peri | Lava | Limp | Clam | |
| 1–4 m | | | | | | |
| Tube | 859 | 228 | 30 | 4 | 2 | 76.5 |
| Peri | 184 | 996 | 166 | 48 | 63 | 68.4 |
| Lava | 3 | 127 | 780 | 28 | 48 | 79.1 |
| Limp | 0 | 8 | 15 | 806 | 250 | 74.7 |
| Clam | 0 | 42 | 27 | 220 | 772 | 72.8 |
| 4–7 m | | | | | | |
| Tube | 373 | 55 | 14 | 0 | 3 | 83.8 |
| Peri | 43 | 271 | 68 | 4 | 6 | 69.1 |
| Lava | 28 | 61 | 176 | 2 | 3 | 65.2 |
| Limp | 0 | 4 | 1 | 231 | 5 | 95.9 |
| Clam | 1 | 9 | 9 | 13 | 119 | 78.8 |
| 7–10 m | | | | | | |
| Tube | 113 | 2 | 0 | 0 | 0 | 98.3 |
| Peri | 2 | 103 | 0 | 1 | 0 | 97.2 |
| Lava | 3 | 0 | 71 | 11 | 0 | 83.5 |
| Limp | 0 | 2 | 15 | 89 | 0 | 84.0 |
| Clam | 0 | 0 | 0 | 0 | 29 | 100.0 |

*Notes:* To construct this table, all available backscatters and variables of the VT data table were used to create the discriminant model and for prediction. The total number of backscatters in the data tables are 5706 for 1–4 m, 1499 for 4–7 m, and 441 for 7–10 m. Partial PCC stands for the percentage of backscatters from a given habitat that were correctly classified by reference to our visual habitat classification.

ues. For the VI variables, Table A2 in Appendix A gives the skewness values calculated for all transformations applied to segments of the altitude transects. Exhibiting the lowest skewness values, the double square-root transformation followed by the arcsine transformation was consistently the most appropriate combination of transformations for VI variables, except for the 7–10 subtable, in which the Hellinger transformation produced a result slightly better than the arcsine transformation. A double square-root followed by an arcsine transformation was consequently applied to all VI data tables (intensities). That transformation implies that only the shape information remains to be analyzed in the transformed VI data tables, since VI variables are ranged by dividing their values by the maximum intensity present in the original signal.

Upon examination of the VI, VE, and VT variables retained after forward selection, the following trends were observed (Appendix A: Table A3). On average, out of 59 VI, 25 VE, and 84 VT available variables, only six, seven, and nine variables, respectively, were retained by forward selection. The frequency distribution of the intensity variables selected in either VI or VT shows that 20% are found between Int1 and Int26, 60% are found between Int26 and Int90, and 20% are found above Int90 (the latter group was never selected at low altitude, 1–4 m). Consequently, inside the group of the most often selected variables (code SEL), a similar ratio was kept: the eight Int variables selected were "Int11–15," "Int21–25," "Int31–35," "Int46–50," "Int55–60," "Int71–75," "Int91–95," and "Int181–185"; for the VE variables retained after VE or VT forward selection, the seven variables with the highest selection frequencies were "DRSx," "Skew," "NewAlt," "Vmn.s," "Histo1," "Vmx.sE1," "Vmx.sE2," and "Time.RE1."

Table 1 shows differences in classification performance among the three types of data tables. Data tables VT led to higher percentages of correct classification than either VI or VE. Table 1 allows us to answer our first question: Is the information found within backscatters informative enough to allow accurate discrimination of abyssal benthic habitats, in this particular case, five hydrothermal habitats within a vent field ecosystem? Using only the sonar samples taken during the stable section of each transect, defined by moments of low altitude where the ROV was minimizing its vertical and horizontal displacements, a control test was performed. Even if the overall efficiency of our method cannot be assessed using only the percentages of correct classification for STB data, the high PCC values (82.9%, 90.5%, and 94.8%) obtained in this controlled situation confirm that the five hydrothermal habitats under study possess differentiable and repeatable sonar signatures.

### *Relationship between PCC and altitude*

To verify the performance of the VI, VE, and VT data tables between 1 and 10 m, we compared the percentages of correct classification for all backscatters (code ALL) to those of the transect with the best backscatter quality (code BEST). The latter gave, on average, 12.7% better results (Table 1). It appears that this subset of variables displayed limited habitat variation in the sonar signatures and consequently facilitated discrimination. In order to understand why, on average, ALL and BEST had such low discrimination capacity (61.7% and 74.4%, respectively) compared with the mean of 89.4% for the low-altitude subtable (code STB), we compared the PCC obtained for altitude-specific subtables (1–4, 4–7, and 7–10 m) to identify how the intrahabitat variation was distributed within our transects. At altitude ranges of 1–4 and 4–7 m, on average, the PCCs obtained were similar, but an increase in PCC averaging 10.7% occurred between 4–7 and 7–10 m.

In an attempt to illustrate why an altitude-related variation can be seen even on depth-normalized data, we compared the classification obtained through sonar signature discrimination with our initial visual habitat classification for the VT data tables. The results in Table 2 provide an answer to our second question: Does increasing footprint size allow the acquisition of echoes that are increasingly representative of the spatial heterogeneity inherent to each habitat? At 1–4 m, 4–7 m, and 7–10 m of altitude, the sonar beam width was respectively 3–12, 12–20, and 20–30 cm in diameter. This means that the very small footprints at low altitude were more likely to detect intrahabitat patches of different textures and densities. For example, the classification obtained for the Peri habitat at 1–4 m shows that, besides the 68.4% of the backscatters that were correctly classified, most of the remaining acoustic returns were classified as representing the Lava and Tube habitats, which are the Peri main constituents. In the classification results obtained for the 1–4 m and the 4–7 m data, a clear division exists between the acoustic returns belonging to the Lava, Peri, and Tube habitats on the one hand and the Limp and Clam habitats on the other. The 4–7 m data do better than the 1–4 m data at separating the Limp and Clam backscatters. At 7–10 m of altitude, most (91.8%) of the sonar signatures were correctly classified, indicating that an optimal footprint size had been reached.

## Technical Discussion

### *The influence of altitude*

Having shown (Fig. 4) that an accurate depth normalization was applied on all backscatters, because the footprint size of the sonar beam is directly related to the ROV altitude by physical laws, the variable "NewAlt" describing the ROV altitude was used to monitor the impact of footprint size on our discrimination capacity. By looking at the explanatory variables selected to describe the data tables and subtables (Appendix A, Table A3), we realized that in the 7–10 subtables, "NewAlt" was never selected among the significant variables for VE and VT. This absence was attributed to the fact that, as the footprint expands with altitude, the backscatter signals incorporate more and more of the habitat's fine-grain spatial heterogeneity. Therefore, as long as the amount of heterogeneity sampled is not sufficiently representative of a sampled habitat texture and density, the nature of the information in the backscatter is likely to change with altitude. Thus, as long as the sonar has sampled an area representative of the habitat general texture and density, whatever the variation in altitude, the resulting sonar signature variation no longer relates to altitude, producing better discrimination among habitat types.

### *The nature of the five habitat type signatures*

Our third and last question was: Can we find specific sets of variables that could be used to correctly identify the nature of the habitat surveyed, based on sonar signatures? We used the set of selected variables (SEL) to compute discriminant functions among habitat types and produced six graphical representations of the resulting habitat cluster projections on the first and second discriminant axes (Appendix B). From these analyses, the centroids of the habitat clusters were correlated with the environmental variables. The correlations were noted in Table 3 as either positive "+," negative "–," or null "0."

The VE and VI results presented in Table 3 were written to two data files, each with five rows (habitat types) and 24 columns (the rows of Table 3), and analyzed by *K*-means partitioning. For VE and VI as well, the results indicated the presence of two major groups of habitats differentiated by the variables derived from the backscatters: Clam and Limp formed the first group and Lava, Peri, and Tube formed the second. Skewness of the first echo (variable "Skew"), as well as intensity variables "Int31–35," "Int46–50," and "Int71–75" were good indicators of this partition.

1. *Clam and Limp habitats.*—Habitat Clam had the most highly and positively skewed first echo, followed by Limp. The rise section of the first echo was short and correlated with strong intensities whereas the set section had mostly low intensities. Clam's sonar signatures were also negatively correlated to the maximum value of the smoothed first echo (variable "Vmx.sE1"), which indicates the presence of a smooth and soft type of surface (Bax et al. 1999). The positive correlations of the Clam centroid with the minimum value between the two echoes (variable "Vmn.s") indicates that after the first echo, the ambient noise remaining in the signal was higher than for other habitats.

The less strongly skewed signatures of the Limp habitat showed a small amount of low-class intensities (variable "Histo1"), very strong negative correlations with the minimum value between the two echoes (variable "Vmn.s"), and good positive correlations with the maximum value of the smoothed second echo (variable "Vmx.sE2"). These correlations support the idea that the Limp habitat contained high densities of gastropod shells, which produced a very reflective, hard, and smooth surface allowing for low energy penetration. The sonar wave dissipated well, which produced low intensity values between the two echoes (variable "Vmn.s"). An interesting fact about Limp is the differentiation between the rise and set sections of the first echo. As soon as the positively correlated rise section

TABLE 3. Correlation between sonar variables and habitat types, for the three altitude ranges.

| | | Habitat types | | | | | | | Habitat types | | | | |
|---|---|---|---|---|---|---|---|---|---|---|---|---|---|
| VE | Alt. | Tube | Peri | Lava | Limp | Clam | VI | Alt. | Tube | Peri | Lava | Limp | Clam |
| | 1–4 | – | – | 0 | + | + | | 1–4 | – | – | + | + | + |
| DRSx | 4–7 | – | 0 | 0 | + | + | Int11–15 | 4–7 | – | 0 | – | + | 0 |
| | 7–10 | – | + | + | + | – | | 7–10 | 0 | – | + | 0 | 0 |
| | 1–4 | + | + | + | – | – | | 1–4 | 0 | – | + | 0 | 0 |
| Histo1 | 4–7 | + | – | – | – | + | Int21–25 | 4–7 | + | 0 | + | – | + |
| | 7–10 | 0 | 0 | 0 | 0 | 0 | | 7–10 | 0 | + | – | – | + |
| | 1–4 | – | – | 0 | + | + | | 1–4 | + | 0 | + | – | – |
| Skew | 4–7 | – | – | – | + | + | Int31–35 | 4–7 | + | + | + | – | – |
| | 7–10 | – | – | + | 0 | + | | 7–10 | 0 | + | – | 0 | 0 |
| | 1–4 | + | 0 | – | 0 | – | | 1–4 | + | + | – | – | – |
| Time.RE1 | 4–7 | + | 0 | 0 | – | – | Int46–50 | 4–7 | + | + | 0 | – | – |
| | 7–10 | + | + | 0 | 0 | – | | 7–10 | + | + | – | – | 0 |
| | 1–4 | – | 0 | + | – | 0 | | 1–4 | + | + | + | – | – |
| Vmn.s | 4–7 | + | – | – | – | + | Int56–60 | 4–7 | + | + | + | – | – |
| | 7–10 | 0 | – | 0 | – | + | | 7–10 | + | 0 | 0 | – | – |
| | 1–4 | – | + | + | – | – | | 1–4 | + | 0 | + | – | – |
| Vmx.sE1 | 4–7 | 0 | + | + | 0 | – | Int71–75 | 4–7 | + | + | + | – | – |
| | 7–10 | 0 | 0 | 0 | 0 | 0 | | 7–10 | + | 0 | 0 | – | 0 |
| | 1–4 | – | 0 | + | – | 0 | | 1–4 | + | 0 | + | – | – |
| Vmx.sE2 | 4–7 | – | + | + | + | – | Int91–95 | 4–7 | 0 | 0 | 0 | – | + |
| | 7–10 | 0 | 0 | 0 | + | 0 | | 7–10 | + | 0 | 0 | – | – |
| | 1–4 | 0 | 0 | 0 | 0 | 0 | | 1–4 | 0 | 0 | + | 0 | 0 |
| NewAlt | 4–7 | + | + | + | 0 | – | Int181–185 | 4–7 | 0 | – | 0 | – | + |
| | 7–10 | 0 | 0 | 0 | 0 | 0 | | 7–10 | – | + | – | 0 | + |

*Notes:* The table reports correlations of selected environmental variables with the centroids of the five habitat types in the space of the first two discriminant functions for the various altitude subtables: 1–4, 4–7, and 7–10 m. Positive, negative, and uncertain correlations are marked, respectively, as "+," "–," and "0." The "0" case occurred when the habitat centroid was at an angle close to 90° with the variable vector or when the variable was considered unstable based on its canonical weight and correlation vectors, shown in panels (a) and (b) of Figs. B1–B6 of Appendix B. For each habitat, the variables showing the same correlation sign over the three altitude classes are highlighted in dark gray; those that only have two identical signs out of three are highlighted in light gray. In the left-hand half of the table, height echo shape variables (VE) are used. DRSx corresponds to the time distance between rise and set area centroids of the first echo (E1). Out of a seven-class histogram describing E1 intensities based on matrix max, Histo1 is the first class. Skew is the E1 skewness, which is derived from the third statistical moment. Time.RE1 is the time proportion between E1 rise and E1 total time laps. Vmn.s is the minimum value found between smoothed E1 and second echo (E2). Vmx.sE1 is the maximum value in the smoothed E1. Vmx.sE2 is the maximum value in the smoothed E2, and NewAlt is the echo acquisition altitude. In the right-hand half of the table, height power intensity variables (VI) are used. Their number simply defines which echo intensity values were averaged to produce the given variable. More details are given about VE variables in Table A1 of Appendix A; see Fig. 3 for a visual representation of the VI variables.

passed the "Int11–15" intensity variable, negative correlations appeared from that point until the end of the set section (variable "Int91–95").

2. *Tube, Peri, and Lava habitats.*—In the group with the most negatively skewed first echoes, the Tube habitat was the most extreme, followed by Peri sonar signatures. In both cases, the echo shapes were the opposite of Clam and Limp. Their intensity variable correlations described a slow rise section, followed by higher intensities in the set section. While the Peri signature presented positive correlations in the set section of the first echo until variable "Int56–60," the Tube correlations were positive until "Int91–95"; they were more stable in the sense that they were found more often in the entire 1–10 m altitude range. This suggests that, as the density of tubeworms increased, the first echo became longer since the positive correlations with intensity variables went further to the right in the set section. Beside the fact that the Tube's first echo intensities could be described by low intensities, they were shaped by numerous peaks and troughs. The positive correlations with variable "Histo1" and negative correlations with "Vmx.sE2" indicate how weak the sonar signal became after multiple reflections around the uneven and smooth tubular structures of the tubeworms.

Lava represented an intermediate case between the Tube and Clam extremes. In terms of correlations, Peri sonar signatures were intermediates between the Lava and Tube signatures. Obviously affected by the presence of the relatively rough and hard lava surface within its habitat, most of the strong correlations seen in Tube, such as with "Skew," "DRSx," "Histo1," or in Lava with "Vmx.sE1," were weaker in the Peri habitat. The Lava sonar signatures correlated with a quick rise and a set section that showed positive correlations reaching up to "Int71–75." It was also the habitat associated with the strongest smoothed maximum in the first echo. The high-intensity set section of Lava might relate to the fact that most Lava reflections were influenced by the unevenness of the broken lava sheets.

## Conclusion

Besides surface roughness and hardness, many factors such as sonar signal frequency, ping length, and beam width (footprint) can affect echo shapes. One of the major issues in backscatter analysis is the use of correct depth normalization procedures (Hamilton 2001). To properly study the reflective nature of each habitat, we must ensure that most of the altitude-related variation is removed prior to analysis. The visual representation of that correction, such as in our Fig. 4, is quite important because it allows an assessment of the procedure used.

Under the assumption of an accurate depth normalization procedure, the presence of the "NewAlt" variable among the variables retained by forward selection would indicate the influence of footprint size variation. "NewAlt" was not selected to describe any of the 7–10 m data tables (Appendix A: Table A3). That, and the stronger discrimination shown by the 7–10 m tables compared to the other depths (Table 2), led us to conclude that footprint size can drastically affect our capacity to investigate and ultimately detect habitat types.

Prior to any sonar survey, it is essential to make sure that the sonar settings are optimal. We used vertical transects over identifiable habitat types to verify the sonar's ability to differentiate the five habitats under investigation. This exercise permitted the identification of key variables derived from backscatters and allowed us to identify an optimal footprint size to achieve sampling at scales that are representative of the general habitat textures and densities. Having optimized the sonar acquisition settings and depth normalization procedure, to bring even more robustness to sonar surveys, new sonar technology will need to be developed to allow the footprint size to remain constant during seafloor classification surveys (Legendre et al. 2002). Even when that technology becomes available, we will still be a long way from developing databases of sonar signature definitions describing diverse habitat types found over whole benthic ecosystems. To construct such a database would require each habitat to be described using a constant set of variables based on various and specific sets of frequencies, footprint sizes, and pulse lengths. Before such standardization can be initiated, more work will be required to identify the best frequency combinations and sets of explanatory variables.

In this paper, we have shown that abyssal habitat identification is possible through the use of sonar signatures based on only one frequency, using a small and changing footprint and using a remotely operated vehicle operating at 2200 m deep. This provides some optimism for future sonar mapping developments. Multiscale high-resolution seafloor sonar surveys may prove very useful for habitat mapping, resource evaluation, and ecosystem management purposes.

Before sonar-based systems can be used routinely for broad-scale surveys of habitats, many issues remain to be addressed both in terms of the sonar signal frequencies to be used and the establishment of key variable sets. Bax et al. (1999:717) wrote: ". . . it is clear that the full power of acoustic habitat discrimination has not yet been realized—there is far more information in the returning echoes and the pattern of echoes than is currently being interpreted."

Sonar remote-sensing surveys require both a set of sonar signatures and some ground truthing, the latter through either visual investigation or physical sampling, both of which are highly time consuming. The need for ground truthing could be reduced through the development of a database on the behavior of sonar signatures in various types of substrata and habitats through a series of criteria spreading over ranges of specific frequencies and sampling unit sizes (grain size). The development of such a database would require cooperation between researchers and the companies providing benthic remote-sensing services. In order to encourage free and open communication and debate, we provide the definitions of our variables in Appendix A for scrutiny and use by the scientific research and technology communities.

The sonar variables developed in this study and the method for extracting and transforming them are fully described in this paper and are available in the public domain.

### *Technical implications for other domains*

Classical remote-sensing methods are extensively used to produce bathymetric maps describing the demersal relief found in any type of water body. In these surveys, variables describing the echo time of arrival, such as "NewAlt," are used to compute altitude, which is, when added to the sonar depth, the information illustrated in bathymetric maps. With variables such as the echo general power intensity, e.g., "Vmx.sE1," texture and density layers can be overlaid over bathymetric maps for substrate type identification. Extending the domain of application further, the method presented in this paper can be used as a guide for those who either wish to extract more information from remote sonar surveys, find other useful variables to extract, or use new sonar frequencies. The science behind understanding sonar signatures is young, but it has potential applications in fine- to broad-scale ecological surveys serving monitoring, management, and exploration purposes. Fish school identification capabilities could be improved by using some of the sonar variables described in this paper. Beyond the realm of aquatic sciences, sonar signatures can be used in many terrestrial applications. Mobile robots, which are already extensively using ultrasounds, have external sensors; a fine analysis of the sound returns in detection algorithm would give robots another mean to identify the nature of the objects they encounter.

## Acknowledgments

This work would not have been possible without the dedication of the ROPOS submersible pilots and the crewmembers of the CCGS John P. Tully. This research was sponsored by NSERC (Canada) Collaborative Research Opportunities grants to S. K. Juniper and P. Legendre, and by the Canadian Scientific Submersible Facility. We are particularly grateful to L. J. Hamilton (backscatter analysis), S. Dray (R language and statistical analysis), M. Fellows (Imagenex surveys), Imagenex Corporation (post-processing support), and J. Illman (navigation software training) for advice and help. We also benefited from interesting comments by two anonymous reviewers.

## Literature Cited

Bax, N. J., R. J. Kloser, A. Williams, K. Gowlett-Holmes, and T. Ryan. 1999. Seafloor habitat definition for spatial management in fisheries: a case study on the continental shelf of southeast Australia. Oceanologica Acta **22**:705–720.

Brown, C. J., K. M. Cooper, W. J. Meadows, D. S. Limpenny, and H. L. Rees. 2002. Small-scale mapping of sea-bed assemblages in the eastern English Channel using sidescan sonar and remote sampling techniques. Estuarine, Coastal and Shelf Science **54**:263–278.

Burczynski, J. 2001. Bottom classification. Biosonics, Seattle, Washington, USA.

Burns, D. R., C. B. Queen, H. Sisk, W. Mullarkey, and R. C. Chivers. 1989. Rapid and convenient acoustic sea-bed discrimination for fisheries applications. Proceedings of the Institute of Acoustics **11**:169–178.

Carey, D. A., D. C. Rhoads, and B. Hecker. 2003. Use of laser line scan for assessment of response of benthic habitats and demersal fish to seafloor disturbance. Journal of Experimental Marine Biology and Ecology **285–286**:435–452.

Chivers, R. C., N. Emerson, and D. R. Burns. 1990. New acoustic processing for underway surveying. Hydrographic Journal **56**:9–17.

Clarke, P. A., and L. J. Hamilton. 1999. The ABCS Program for the analysis of echo sounder returns for acoustic bottom classification. DSTO-GD-0215. Defence Science and Technology Organisation, Aeronautical and Maritime Research Laboratory, Melbourne, Victoria, Australia.

Durand, S., M. Le Bel, S. K. Juniper, and P. Legendre. 2002. The use of video surveys, a geographic information system and sonar backscatter data to study faunal community dynamics at Juan de Fuca Ridge hydrothermal vents. Cahiers de Biologie Marine **43**:235–240.

Ellingsen, K. E., J. S. Gray, and E. Bjørnbom. 2002. Acoustic classification of seabed habitats using the QTC VIEW system. Journal of Marine Sciences **59**:825–835.

Foster-Smith, R. L., and I. S. Sotheran. 2003. Mapping marine benthic biotopes using acoustic ground discrimination systems. International Journal of Remote Sensing **24**:2761–2784.

Hamilton, L. J. 2001. Acoustic seabed classification systems. DSTO-TN-0401. Defense Science and Technology Organisation, Aeronautical and Maritime Research Laboratory, Fishermans Bend, Victoria, Australia.

Hewitt, J. E., S. F. Thrush, P. Legendre, G. A. Funnell, J. Ellis, and M. Morrison. 2004. Mapping of marine soft-sediment communities: integrated sampling for ecological interpretation. Ecological Applications **14**:1203–1216.

Irish, J. L., and W. J. Lillycrop. 1999. Scanning laser mapping of the coastal zone: the SHOALS system. Journal of Photogrammetry and Remote Sensing **54**:123–129.

Kotchenova, S. T., X. Song, N. V. Shabanov, C. S. Potter, Y. Knyazikhin, and R. B. Myneni. 2004. Lidar remote sensing for modeling gross primary production of deciduous forests. Remote Sensing of Environment **92**:158–172.

Lee, K.-H., and E. N. Anagnostou. 2004. A combined passive/active microwave remote sensing approach for surface variable retrieval using Tropical Rainfall Measuring Mission observations. Remote Sensing of Environment **92**:112–125.

Lee, S. H., and S. K. Chough. 2001. High-resolution (2–7 kHz) acoustic and geometric characters of submarine creep deposits in the South Korea Plateau, East Sea. Sedimentology **48**:629–644.

Legendre, P., K. E. Ellingsen, E. Bjørnbom, and P. Casgrain. 2002. Acoustic seabed classification: improved statistical method. Canadian Journal of Fisheries and Aquatic Sciences **59**:1085–1089.

Léveillé, R. J., and S. K. Juniper. 2003. Biogeochemistry of deep-sea hydrothermal vents and cold seeps. Pages 238–292 *in* K. D. Black, and G. B. Shimmield, editors. Biogeochemistry of marine systems. Blackwell, Sheffield, UK.

Moya, I., L. Camenen, S. Evain, Y. Goulas, Z. G. Cerovic, G. Latouche, J. Flexas, and A. Ounis. 2004. A new instrument for passive remote sensing. 1. Measurements of sunlight-induced chlorophyll fluorescence. Remote Sensing of Environment **91**:186–197.

Pace, N. G., and H. Gao. 1988. Swathe seabed classification. Journal of Oceanic Engineering **13**:83–90.

Parry, D. M., M. A. Kendall, D. A. Pilgrim, and M. B. Jones. 2003. Identification of patch structure within marine benthic landscapes using a remotely operated vehicle. Journal of Experimental Marine Biology and Ecology **285–286**:497–511.

Prager, B. T., D. A. Caughey, and R. H. Poeckert. 1995. Bottom classification: operational results from QTC view. Pages 1827–1835 *in* Oceans'95 MTS/IEEE—Challenges of Our Changing Global Environment Conference Proceedings 9–12 October 1995. Volume 3. MTS/IEEE, San Diego, California, USA.

R Development Core Team. 2005. R: a language and environment for statistical computing. R Foundation for Statistical Computing, Vienna, Austria. ⟨http://www.R-project.org⟩

Sarrazin, J., and S. K. Juniper. 1999. Biological characteristics of a hydrothermal edifice mosaic community. Marine Ecology Progress Series **185**:1–19.

Schmidtlein, S., and J. Sassin. 2004. Mapping of continuous floristic gradients in grasslands using hyperspectral imagery. Remote Sensing of Environment **92**:126–138.

ter Braak, C. J. F., and P. Smilauer. 2002. CANOCO reference manual and CanoDraw for Windows user's guide: software for canonical community ordination. Version 4.5. Microcomputer Power, Ithaca, New York, USA.

Tsurumi, M., and V. Tunnicliffe. 2003. Tubeworm-associated communities at hydrothermal vents on the Juan de Fuca Ridge, northeast Pacific. Deep-Sea Research **50**:611–629.

Wirsen, C. O., S. M. Sievert, C. M. Cavanaugh, S. J. Molyneaux, A. Ahmad, L. T. Taylor, E. F. DeLong, and C. D. Taylor. 2002. Characterization of an autotrophic sulfide oxidizing marine *Arcobacter* sp. that produces filamentous sulfur. Applied and Environmental Microbiology **68**:316–325.

Zajac, R. N., R. S. Lewis, L. J. Poppe, D. C. Twichell, J. Vozarik, and M. L. DiGiacomo-Cohen. 2003. Responses of infaunal populations to benthoscape structure and the potential importance of transition zones. Limnology and Oceanography **48**:829–842.

## APPENDIX A

Three tables showing (1) the definitions of the variables describing echo shapes along with the transformation details, (2) transformation trials for the intensity variables data, and (3) the variables retained by forward selection (*Ecological Archives* A016-047-A1).

## APPENDIX B

Figures showing habitat clusters that were obtained from different altitude ranges using the variables with the highest selection frequencies (SEL variable subset) projected on the first and second discriminant axes (*Ecological Archives* A016-047-A2).

## SUPPLEMENT

Package for data analysis of echoes used in this study and a sample data set (*Ecological Archives* A016-047-S1).

*Appendices to:*

Sébastien Durand, Pierre Legendre, and S. Kim Juniper. 2006. Sonar backscatter differentiation of dominant macrohabitat types in a hydrothermal vent field. *Ecological Applications* 16:1421–1435.

## APPENDIX A

## *Ecological Archives* A016-047-A1

## THREE TABLES SHOWING (1) THE DEFINITIONS OF THE VARIABLES DESCRIBING ECHO SHAPES ALONG WITH THE TRANSFORMATION DETAILS, (2) TRANSFORMATION TRIALS FOR THE INTENSITY VARIABLES DATA, AND (3) THE VARIABLES RETAINED BY FORWARD SELECTION.

Table A1 shows the definitions of the VE variables along with the transformation details, Table A2 the transformation trials for the VI data, and Table A3 the variables retained by forward selection.

TABLE A1. Definitions, transformations, and skewness values of the VE variables (variables describing echo shapes).

| Variable name | Definition | Transformation | Skewness |
|---|---|---|---|
| NewAlt | The computed altitude | Double Sqrt | 1.29 |
| Pmx.sE1 | Point of maximum found in the smoothed E1 | Double Sqrt | 1.24 |
| Pmn.s | Point of minimum found between smoothed E1 and E2 | Sqrt | 1.26 |
| Pmx.sE2 | Point of maximum found in the smoothed E2 | Double Sqrt | 1.36 |
| Vmx.sE1 | Maximum value in the smoothed E1 | None | 0.09 |
| Vmn.s | Minimum value found between smoothed E1 and E2 | Double Sqrt | 3.48 |
| Vmx.sE2 | Maximum value in the smoothed E2 | Double Sqrt | 4.18 |
| DRSx | Time distance between rise and set area centroids of E1 | None | 0.72 |
| DRSy | Intensity distance between rise and set area centroids of E1 | None | 0.14 |
| Area.R | Area below the curve of E1 rise section | Double Sqrt | 1.60 |
| Area.S | Area below the curve of E1 set section | Double Sqrt | 1.48 |
| Area.E2 | Area below the curve of E2 rise section | Double Sqrt | 11.78 |
| Area.RE1 | Proportion between E1 rise and E1 total area | None | 0.10 |
| Area.RE2 | Proportion between E1 rise and E2 rise area | Double Sqrt | 49.80 |
| Time.R | Time laps of E1 rise section | Sqrt | 1.15 |
| Time.S | Time laps of E1 set section | Double Sqrt | 2.06 |

| | | | |
|---|---|---|---|
| Time.E2 | Time laps of E2 rise section | Double Sqrt | 4.79 |
| Time.RE1 | Proportion between E1 rise and E1 total time laps | Log | 0.26 |
| Time.RE2 | Proportion between E1 rise and E2 rise time laps | Double Sqrt | 6.72 |
| Var | E1 variance (second statistical moment) | Double Sqrt | 2.25 |
| Skew | E1 skewness (derived from third statistical moment) | Log | 0.20 |
| Histo1 | 1st histogram class of E1 intensities, based on matrix max | Double Sqrt | 1.60 |
| Histo2 | 2nd histogram class of E1 intensities, based on matrix max | Double Sqrt | 1.07 |
| Histo3 | 3rd histogram class of E1 intensities, based on matrix max | Log | 0.58 |
| Histo4 | 4th histogram class of E1 intensities, based on matrix max | Double Sqrt | 2.28 |
| Histo5 | 5th histogram class of E1 intensities, based on matrix max | Double Sqrt | 13.94 |
| Histo6 | 6th histogram class of E1 intensities, based on matrix max | Double Sqrt | 32.86 |
| Histo7 | 7th histogram class of E1 intensities, based on matrix max | Double Sqrt | 69.48 |

*Notes*: The VE variables used in our analyses were selected out of a larger set of 66 variables in such way as to minimize collinearity among the variables. Then, out of four transformations (none, log, sqrt, and double sqrt), the transformation producing the lowest skewness values was applied to each of these variables. For all rising, setting, and complete sections found in our backscatters, the areas under the curves and the time spent were calculated. The following area and time spent proportions were also calculated: E1 rise / E1 complete and E1 rise / E2 rise. The points and values of maximum intensity found in E1 and E2, in both the original and smoothed curves, and the point and value of minimum intensity found between these maxima were also described. Finally, the statistical moments, a 7-class histogram of E1 intensity values, and the distances in the x and y directions, between the centroids of the E1 rising and setting sections, were calculated.

TABLE A2. Transformation trials for the VI data table and subtables.

| Table types | First transformation | Second transformation: None | Arcsine | Hellinger | Table types | First transformation | Second transformation: None | Arcsine | Hellinger |
|---|---|---|---|---|---|---|---|---|---|
| STB | None | 2.05 | 1.30 | 1.05 | 1–4 m | None | 10.62 | 7.70 | 7.49 |
| | Sqrt | 1.07 | 0.69 | 0.57 | | Sqrt | 7.51 | 6.06 | 5.82 |
| | Double Sqrt | 0.69 | **0.44** | 0.62 | | Double Sqrt | 5.95 | **5.51** | 5.58 |
| | Log | 1.93 | — | — | | Log | 10.51 | — | — |
| | Mod. Arcsine | 1.13 | — | — | | Mod. Arcsine | 7.57 | — | — |
| BEST | None | 6.04 | 3.96 | 3.81 | 4–7 m | None | 4.66 | 3.32 | 3.09 |
| | Sqrt | 3.82 | 2.75 | 2.61 | | Sqrt | 3.14 | 2.58 | 2.48 |
| | Double Sqrt | 2.65 | **2.40** | 2.55 | | Double Sqrt | 2.50 | **2.37** | 2.56 |
| | Log | 5.96 | — | — | | Log | 4.61 | — | — |
| | Mod. Arcsine | 3.86 | — | — | | Mod. Arcsine | 3.15 | — | — |
| ALL | None | 13.47 | 8.89 | 8.52 | 7–10 m | None | 3.06 | 2.32 | 2.17 |
| | Sqrt | 8.79 | 6.66 | 6.31 | | Sqrt | 2.19 | 1.87 | 1.70 |
| | Double Sqrt | 6.50 | **5.99** | 6.09 | | Double Sqrt | 1.74 | 1.68 | **1.66** |
| | Log | 13.36 | — | — | | Log | 3.03 | — | — |
| | Mod. Arcsine | 8.86 | — | — | | Mod. Arcsine | 2.21 | — | — |

*Notes:* The presented values are the means of all skewness values computed on all VI data tables after different sequences of transformations. The lowest (best) skewness value for each data subset is in bold. Illogical transformations were not calculated (—). In the first set of transformation, either no transformation (None) was applied, or the effect of high intensity outliers on the distribution was reduced through a square root (Sqrt), double square root (Double Sqrt), log (Log), or modified arsine transformation (Mod.Arcsine). This modified form used the table maximum as the denominator in the calculation of proportions, prior to computing the square root and then the arcsine, instead of the object's maximum in the ordinary arcsine transformation (Sokal and Rohlf 1995). With this modification, all these transformations conserved both the strength and shape information found in backscatters. In a second step, on all the newly transformed tables, we performed either no transformation (None), an ordinary arcsine transformation (Arcsine: $\arcsin(y/y_{max})^{0.5}$), Sokal and Rohlf 1995), or a Hellinger transformation (Hellinger: Legendre and Gallagher 2001). The last two removed the overall intensity of the signal and preserved only the shape information of the sonar returns. STB, BEST, 1–4 m, 4–7 m, and 7–10 m are subtables of ALL, which refers to the complete data set. The STB subtable contained only the echoes acquired while the visibility was optimal and the remotely operated vehicle was in a stable position, hovering at low altitude over the selected habitat. The BEST subtable contained only the best transect for each habitat type. The 1–4 m, 4–7 m, and 7–10 m subtables contained echoes acquired at different altitude ranges, respectively 1 to 4, 4 to 7, and 7 to 10 m.

TABLE A3. Variables retained by forward selection, making the FWD variable sets.

| Method | Table type | Selected variables |
|---|---|---|
| VI | STB | Int46-50, Int26-30, Int81-85, Int41-45, Int71-75, Int1-5, Int11-15, Int31-35 |
| | BEST | Int61-65, Int31-35, Int91-95, Int21-25 |
| | ALL | Int51-55, Int71-75, Int26-30, Int41-45, Int11-15 |
| | 1–4 m | Int55-60, Int41-45, Int71-75, Int26-30, Int11-15 |
| | 4–7 m | Int51-55, Int26-30, Int171-175, Int6-10, Int101-105 |
| | 7–10 m | Int181-185, Int31-35, Int56-60, Int11-15, Int96-100, Int186-190, Int206-210 |
| VE | STB | Skew, Vmn.s, NewAlt, Histo1, Pmn.s, Time.R, Time.RE1, Histo4, Time.S, DRSx |
| | BEST | DRSx, Vmx.sE1, Vmx.sE2, NewAlt, Var |
| | ALL | Skew, Vmn.s, Pmx.sE1, NewAlt, Vmx.sE2, DRSx |
| | 1–4 m | DRSx, Vmn.s, Pmx.sE1, Vmx.sE2, Skew, NewAlt, Histo1 |
| | 4–7 m | Skew, Histo1, Vmx.sE2, Time.RE1, Pmx.sE2, DRSx, Pmn.s |
| | 7–10 m | Histo1, Skew, DRSx, Vmx.sE1, Time.RE1, Time.R, Time.S |
| VT | STB | Int46-50, Int26-30, Vmn.s, Int71-75, NewAlt, Skew, Int1-5, Int41-45, Int81-85, DRSx, Int16-20, Pmn.s |
| | BEST | DRSx, Int31-35, Vmx.sE2, Vmx.sE1, NewAlt, Int91-95 |
| | ALL | Int51-55, Vmn.s, DRSx, Vmx.sE1, Int71-75, Int41-45, Pmx.sE1, Histo2 |
| | 1–4 m | Int56-60, Vmn.s, Skew, Int41-45, Int21-25, Vmx.sE2, Int71-75, Pmx.sE1 |
| | 4–7 m | Skew, Int6-10, DRSx, Int26-30, Int171-175, NewAlt, Int106-110, Int51-55, Int21-25, Vmx.sE2, Vmn.s |
| | 7–10 m | Int181-185, Skew, DRSx, Int31-35, Int71-75, Vmx.sE1, Time.R, Int291-295, Time.RE1 |

*Notes*: The STB, BEST, 1–4, 4–7, and 7–10 subtables are described in the notes of Table A2. Based on their appearance frequencies, the VE variables “DRSx”, “Histo1”, “Skew”, “time.RE1”, “Vmn.s”, “Vmx.sE1”, “Vmx.sE2”, “Newalt” were selected to be included in the SEL variable set. For the VI set, the distribution of the variables selected by forward selection showed that 20% of the variables were describing the rise area of the first echo, and 60% for the set area. Consequently, based on these ratios and on the variable appearance frequencies, “Int11-15”, “Int21-25”, “Int31-35”, “Int46-50”, “Int56-60”, “Int71-75”, “Int91-95”, and “Int181-185” were also selected to be part of set SEL.

## LITERATURE CITED

Legendre, P., and E. D. Gallagher. 2001. Ecologically meaningful transformations for ordination of species data. Oecologia 129:271–280.

Sokal, R. R., and F. J. Rohlf. 1995. Biometry – The principles and practice of statistics in biological research. Third edition. W. H. Freeman, New York, New York, USA.

*Appendices to:*

Sébastien Durand, Pierre Legendre, and S. Kim Juniper. 2006. Sonar backscatter differentiation of dominant macrohabitat types in a hydrothermal vent field. *Ecological Applications* 16:1421–1435.

# APPENDIX B

## *Ecological Archives* A016-047-A2

## FIGURES SHOWING HABITAT CLUSTERS THAT WERE OBTAINED FROM DIFFERENT ALTITUDE RANGES USING THE VARIABLES WITH THE HIGHEST SELECTION FREQUENCIES (SEL VARIABLE SUBSET) PROJECTED ON THE FIRST AND SECOND DISCRIMINANT AXES.

Habitat clusters, obtained from different altitude ranges using the SEL variable subset, projected on the first and second discriminant axes.

The SEL subset of variables was used to construct the six figures presented in this Appendix. The first three figures (Fig. B1, Fig. B2, Fig. B3) are based on the VI data tables (power intensity values found in the echoes) whereas the following three (Fig. B4, Fig. B5, Fig. B6) on the VE data tables (variables describing echo shapes). VT graphs are not shown since the nature of their variable sets (VI and VE combined) makes it harder to unravel the links and relationships between the variables and the centroids of the habitat clusters created by discriminant analysis (R-Pkg::ade4:Discrimin). In each figure, 4 panels (a to d) and one table (e) are shown. In panels (a) to (d), discriminant axis 1 is the abscissa and axis 2 is the ordinate. Panel (a) shows the canonical weights of the variables; panel (b) shows the variables at angles representing their correlations relative to the first two discriminant axes; in panel (c), the eigenvalues of the first four discriminant axes are shown. Panel (d) shows the sonar return clusters based on their video-assigned habitat types; for each habitat cluster, the nametag is located at the cluster centroid. In panel (e), the classification table compares the habitats assigned by discriminant analysis (columns) to the video-assigned habitats (rows). PCC is the percentage of correct classification. In panels (d), the Limp and Clam habitats are always visually well-separated from the other habitat clusters. The habitat assignations in the contingency tables of Figs. B1, B2, B4, and B5 also differentiate these two major groups. It is only in Figs. B3 and B6, which describe echoes acquired between 7 and 10 m of altitude, that most echoes are correctly assigned.

All selected VI variables described in panels (a) and (b) of Figs. B1 to B3 have, at one altitude range or another, shown a high canonical weight or correlation with one of the axes. This behavior suggests that VI is a good variable set for habitat classification. When the VE variables are used (Figs. B4–B6), the "Skew" and "DRSx" variables, which always have strong correlations and canonical weights with the axes, played influential roles in our discrimination results. They allowed us to identify the sonar signatures of the five dominant habitats found in a hydrothermal vent field, 2200 m below the sea surface.

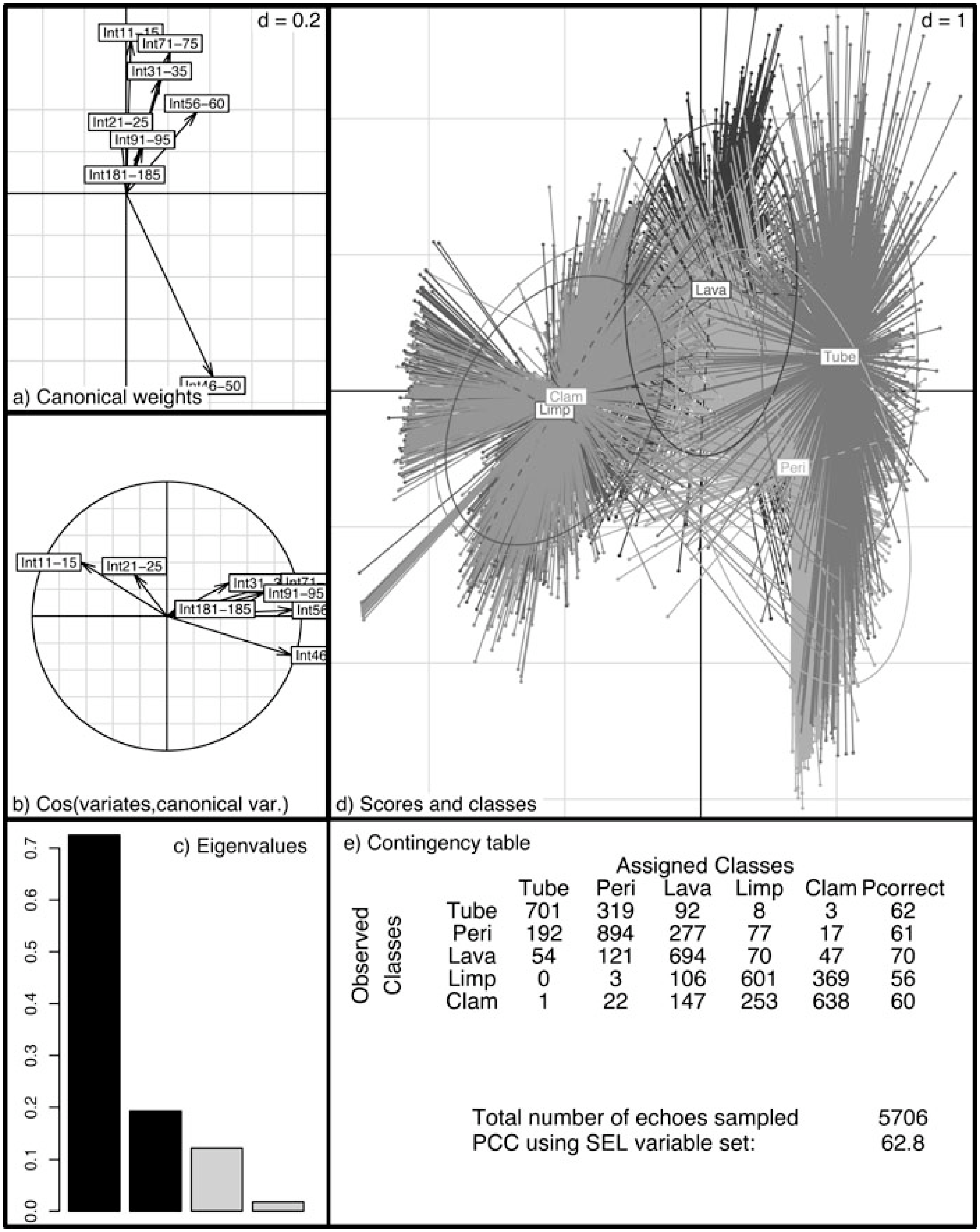


FIG. B1. Table of variables VI, subtable 1–4 m.

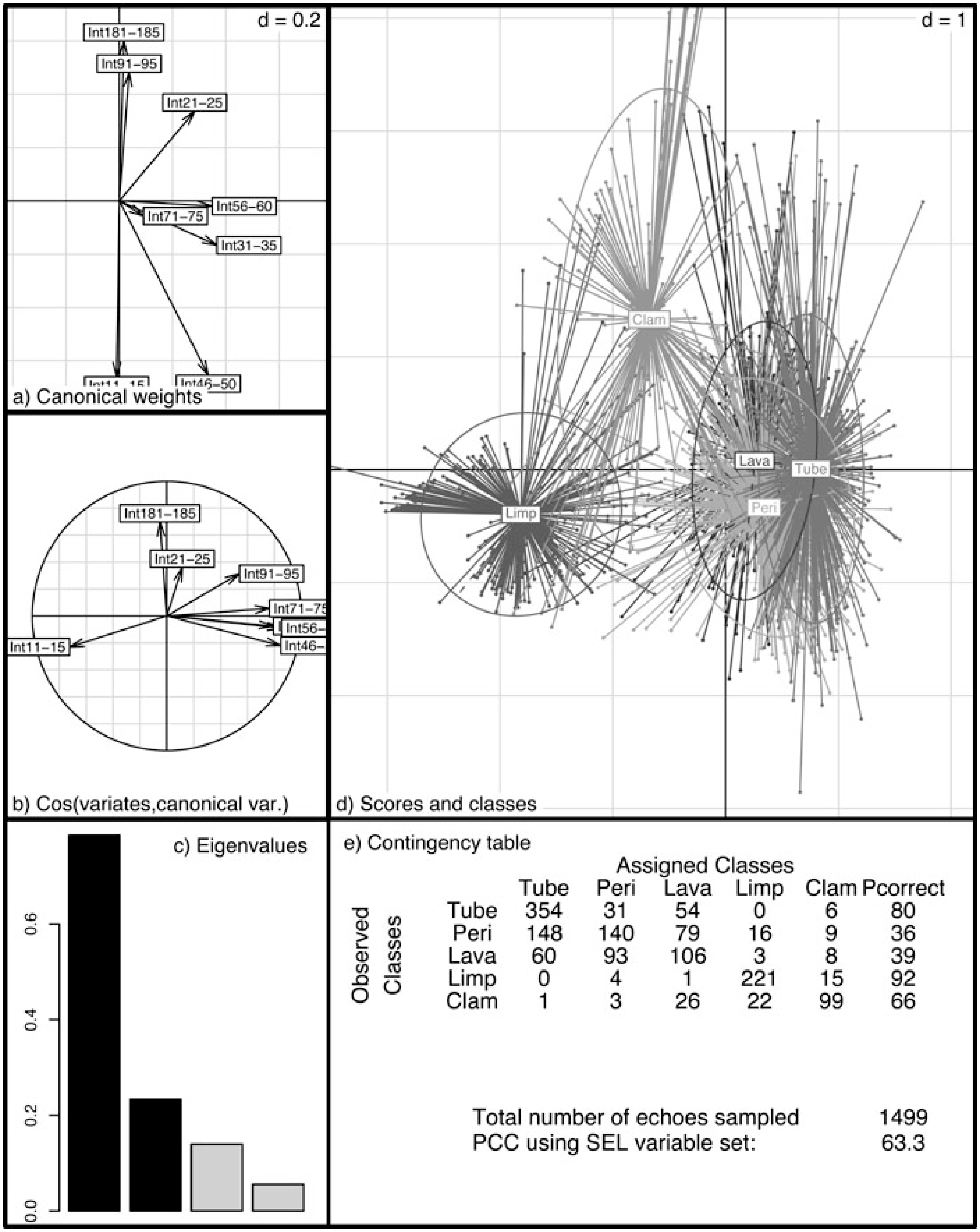


FIG. B2. Table of variables VI, subtable 4–7 m.

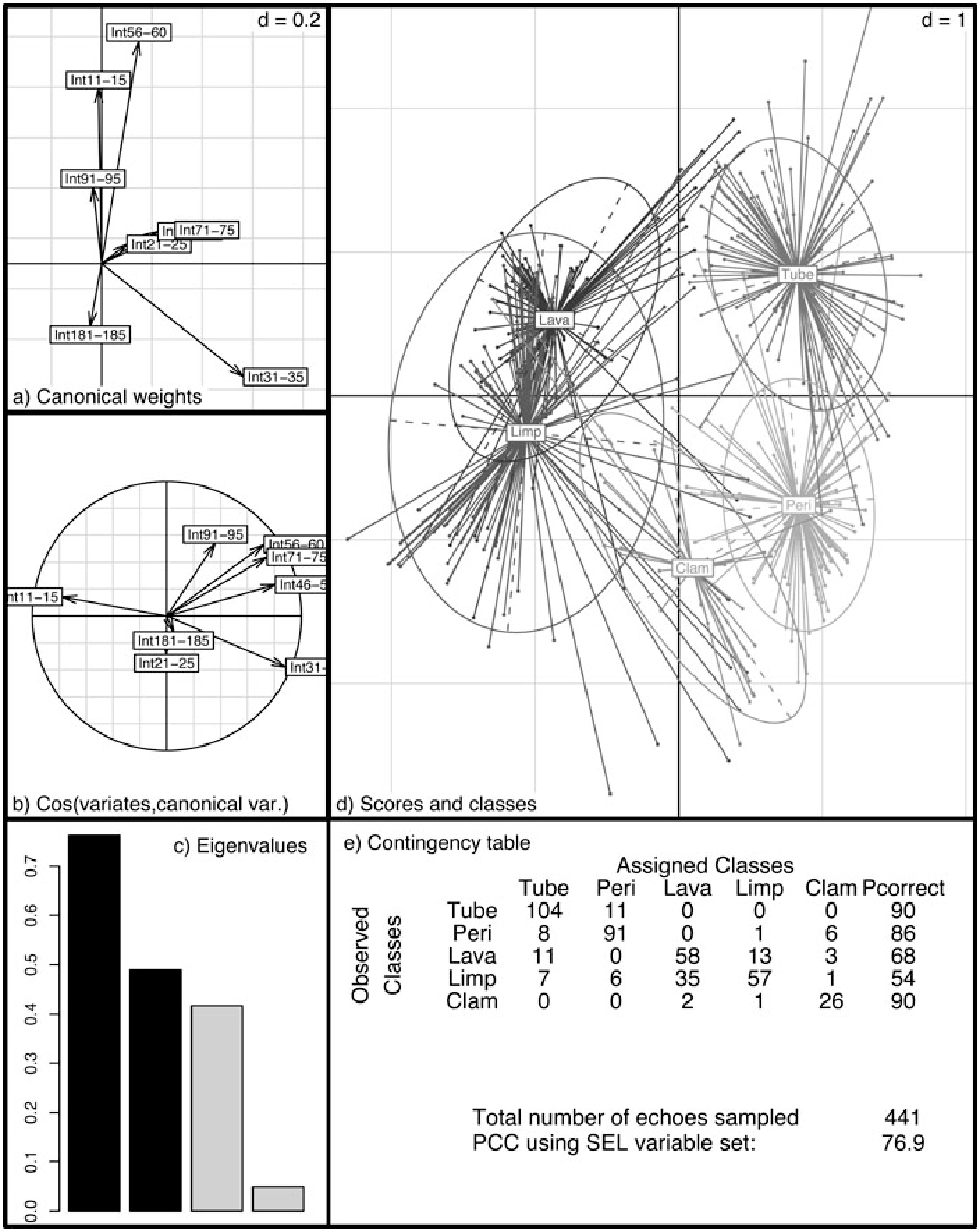


| Observed Classes | Assigned Classes: Tube | Peri | Lava | Limp | Clam | Pcorrect |
|---|---|---|---|---|---|---|
| Tube | 104 | 11 | 0 | 0 | 0 | 90 |
| Peri | 8 | 91 | 0 | 1 | 6 | 86 |
| Lava | 11 | 0 | 58 | 13 | 3 | 68 |
| Limp | 7 | 6 | 35 | 57 | 1 | 54 |
| Clam | 0 | 0 | 2 | 1 | 26 | 90 |

FIG. B3. Table of variables VI, subtable 7–10 m.

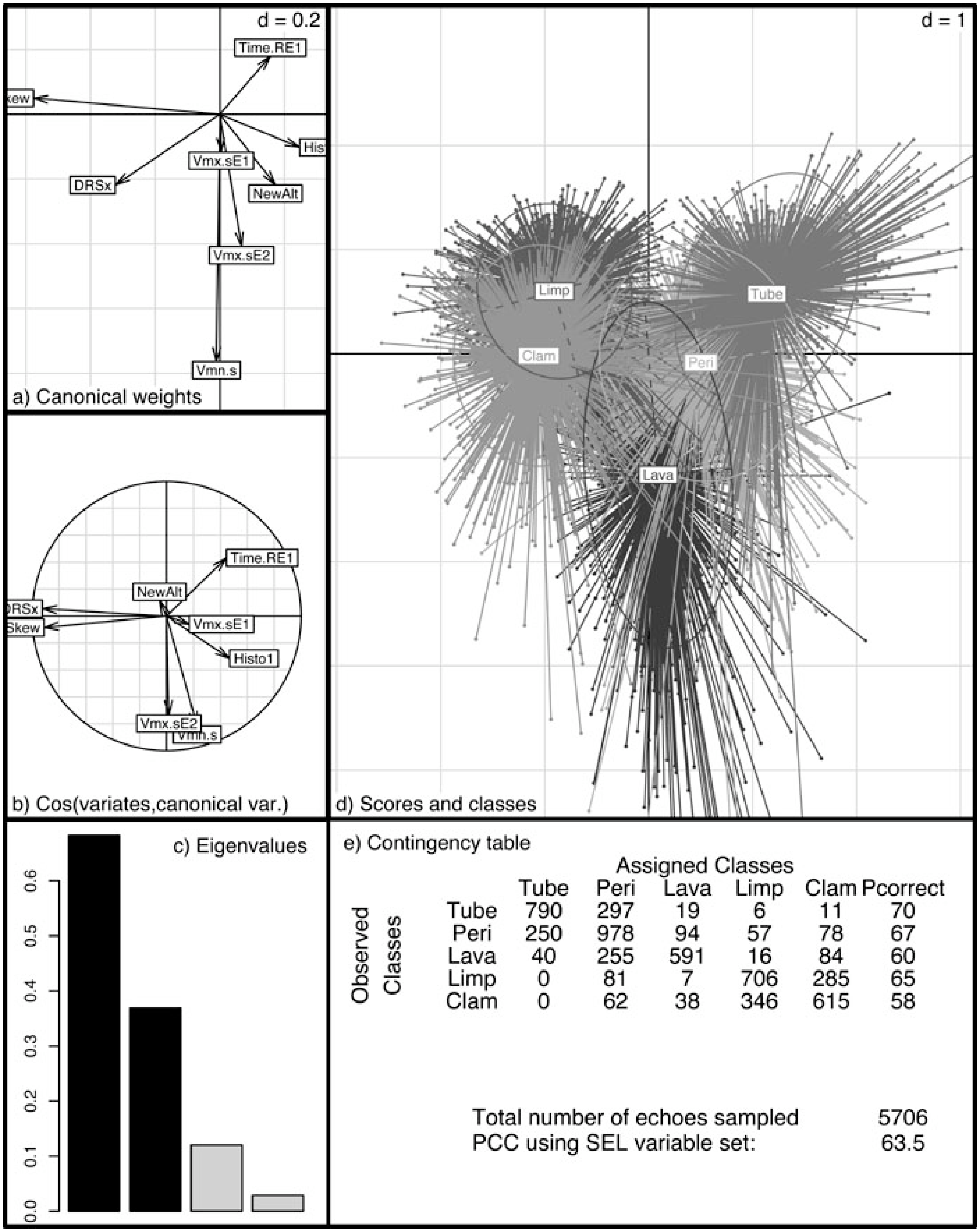


| Observed Classes | Assigned Classes: Tube | Peri | Lava | Limp | Clam | Pcorrect |
|---|---|---|---|---|---|---|
| Tube | 790 | 297 | 19 | 6 | 11 | 70 |
| Peri | 250 | 978 | 94 | 57 | 78 | 67 |
| Lava | 40 | 255 | 591 | 16 | 84 | 60 |
| Limp | 0 | 81 | 7 | 706 | 285 | 65 |
| Clam | 0 | 62 | 38 | 346 | 615 | 58 |

FIG. B4. Table of variables VE, subtable 1–4 m.

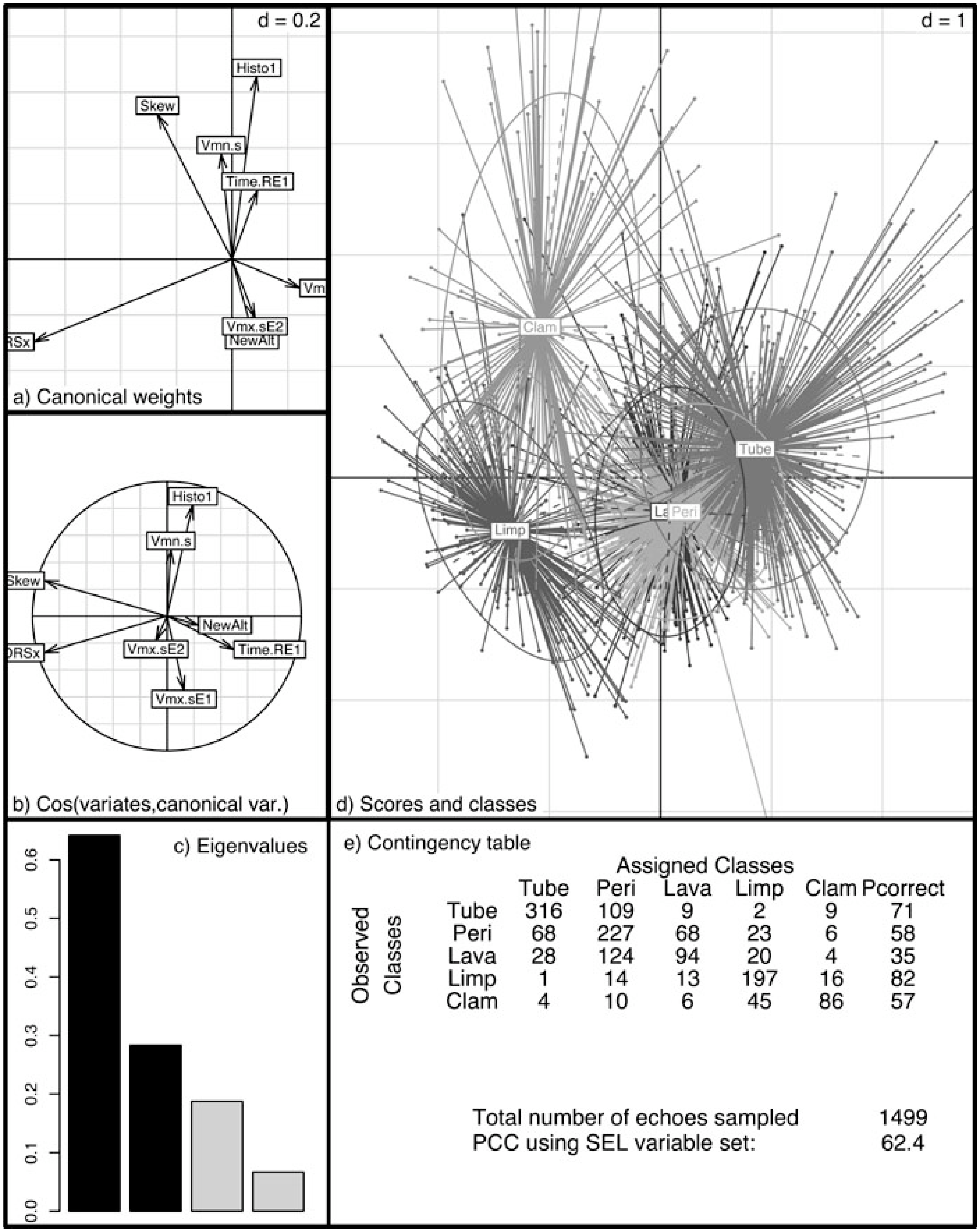


| Observed Classes | Tube | Peri | Lava | Limp | Clam | Pcorrect |
|---|---|---|---|---|---|---|
| Tube | 316 | 109 | 9 | 2 | 9 | 71 |
| Peri | 68 | 227 | 68 | 23 | 6 | 58 |
| Lava | 28 | 124 | 94 | 20 | 4 | 35 |
| Limp | 1 | 14 | 13 | 197 | 16 | 82 |
| Clam | 4 | 10 | 6 | 45 | 86 | 57 |

Total number of echoes sampled 1499
PCC using SEL variable set: 62.4

FIG. B5. Table of variables VE, subtable 4–7 m.

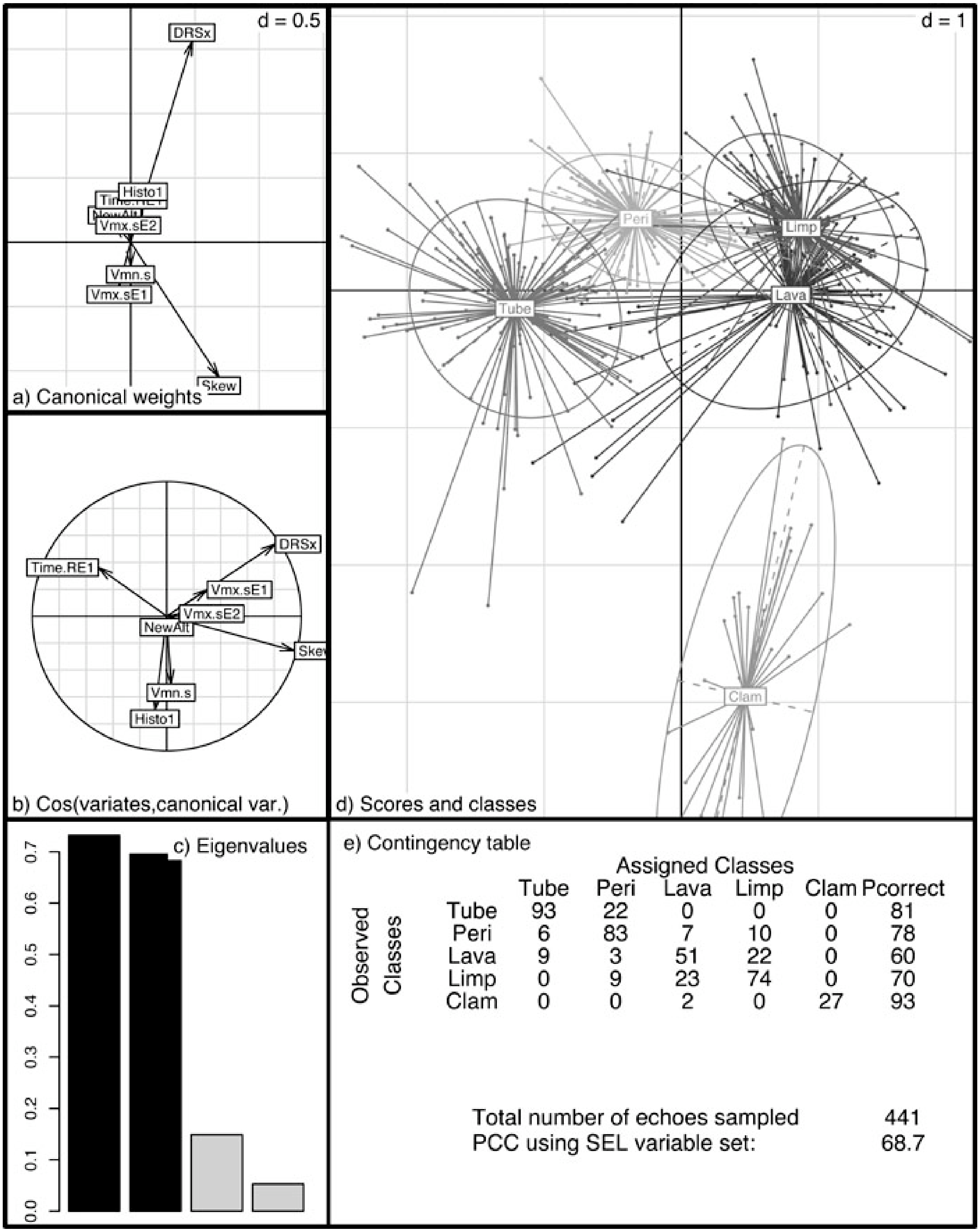


FIG. B6. Table of variables VE, subtable 7–10 m.